Inorg. Chem. **2007**, *46*, 7436–7457

Characterization of the Diradical •NSNSC–CNSSN• and [NSNSC–CNSSN][MF_6]$_n$ (n = 1, 2). The First Observation of an Excited Triplet State in Dimers of 7π –CNSSN• Radicals

Andreas Decken,[†] T. Stanley Cameron,[‡] Jack Passmore,*[,†] J. Mikko Rautiainen,[§] Robert W. Reed,[||] Konstantin V. Shuvaev,[†] and Laurence K. Thompson[⊥]

Department of Chemistry, University of New Brunswick, Fredericton, E3B 6E2, Canada, Department of Chemistry, Dalhousie University, Halifax, B4H 4J3, Canada, Department of Chemistry, University of Jyväskylä, P.O. box 35, 40014, Finland; Department of Chemistry, University of Waterloo, Waterloo, N2L 3G1, Canada, and Department of Chemistry, Memorial University of Newfoundland, St. John's, A1B 3X7, Canada

Received April 3, 2007

Preparation and full characterization of the main-group diradical •NSNSC–CNSSN•, **8**, the MF_6^- salt (As, Sb) of radical cation $^+$NSNSC–CNSSN•, **8**$^{\bullet+}$, and the AsF_6^- salt of the dication $^+$NSNSC–CNSSN$^+$, **8**$^{2+}$, are presented. **8**, a = 6.717 (4), b = 11.701(2), c = 8.269(3) Å, $\alpha = \gamma = 90$, β = 106.69(3)°, monoclinic, space group $P2_1/n$, Z = 4, T = 203 K; **8**SbF_6, a = 6.523(2), b = 7.780(2), c = 12.012(4) Å, α = 91.994(4), β = 96.716(4), γ =109.177(4)°, triclinic, space group $P\bar{1}$, Z = 2, T = 198 K; **8**$[AsF_6]_2$, a = 12.7919(14), b = 9.5760(11), c = 18.532(2) Å, $\alpha = \gamma = 90$, β = 104.034(2)°, monoclinic, space group Pn, Z = 6, T = 198 K. Preparation of **8**MF_6 was carried out via a reduction of $[CNSNS]_2[MF_6]_2$ (M = As, Sb) with either ferrocene or a $SbPh_3$–NBu_4Cl mixture. In the solid state, diamagnetic **8**SbF_6 contains centrosymmetric dimers [**8**$^{\bullet+}$]$_2$ linked via two-electron four-centered π^*–π^* interactions with a thermally excited triplet state as detected by electron paramagnetic resonance (EPR). This is the first observation of a triplet excited state for a 7π 1,2,3,5-dithiadiazolyl radical dimer. The singlet–triplet gap of the [–CNSSN•]$_2$ radical pair was –1800 ± 100 cm^{-1} (–22 ± 1 kJ/mol) with the ZFS components $|D|$ = 0.0267(6) cm^{-1} and $|E|$ = 0.0012(1) cm^{-1}, corresponding to an in situ dimerization energy of ca. –11 kJ/mol. Cyclic voltammetry measurements of **8**$[AsF_6]_2$ showed two reversible waves associated with a stepwise reduction of the two isomeric rings [$E_{1/2}$ (+2/+1) = 1.03 V; $E_{1/2}$ (+1/0) = 0.47 V, respectively]. **8**MF_6 (M = As, Sb) was further reduced to afford the mixed main-group diradical **8**, containing two isomeric radical rings. In solution, **8** is thermodynamically unstable with respect to •NSSNC–CNSSN•, but is isolable in the solid state because of its low solubility in SO_2. Likewise, **8**SbF_6, **8** is dimeric, with π^*–π^* interactions between different isomeric rings, and consequently diamagnetic; however, a slight increase in paramagnetism was observed upon grinding [from C = 6.5(3) × 10^{-4} emu·K/mol and temperature-independent paramagnetism (TIP) = 1.3(1) × 10^{-4} emu/mol to C = 3.2(1) × 10^{-3} emu·K/mol and TIP = 9.0(1) × 10^{-4} emu/mol], accompanied by an increase in the lattice-defect $S = {}^1/_2$ sites [from 0.087(1) to 0.43(1)%]. Computational analysis using the multiconfigurational approach [CASSCF(6,6)/6-31G*] indicated that the two-electron multicentered π^*–π^* bonds in [**8**$^{\bullet+}$]$_2$ and [**8**]$_2$ have substantial diradical characters, implying that their ground states are diradicaloid in nature. Our results suggest that the electronic structure of organic–radical ion pairs, for example, [TTF$^{\bullet+}$]$_2$, [TCNE$^{\bullet-}$]$_2$, [TCNQ$^{\bullet-}$]$_2$, [DDQ$^{\bullet-}$]$_2$, and related π dimers, can be described in a similar way.

1. Introduction

In the last two decades, there has been increasing interest in the synthesis and solid-state properties of heterocyclic thiazyl radicals as precursors to materials with unusual properties, radical-based magnets, and conductors.[1–8] Whereas ring systems **1** and **2** were recognized as better building blocks for conducting materials,[1c,f] two derivatives of radical **3** were found to be ferromagnetic at 1.3 K (R = p-$O_2NC_6F_4$)[3a] and weakly ferromagnetic at 35.5 K (R = p-NCC_6F_4),[3b] Chart 1. Two derivatives of **4** (R = F_3C,[4a] t-Bu[4b,c]) are rare examples of paramagnetic liquids at room temperature. The fused system **5a** has been shown to exhibit optical[5a] and

* To whom correspondence should be addressed. E-mail: passmore@unb.ca; Phone: 1-506-453-4821. Fax: 1-506-453-4981.
[†] Department of Chemistry, University of New Brunswick.
[‡] Department of Chemistry, Dalhousie University.
[§] Department of Chemistry, University of Jyväskylä.
[||] Department of Chemistry, University of Waterloo.
[⊥] Department of Chemistry, Memorial University of Newfoundland.

10.1021/ic700638n CCC: $37.00
Published on Web 08/01/2007

Chart 1

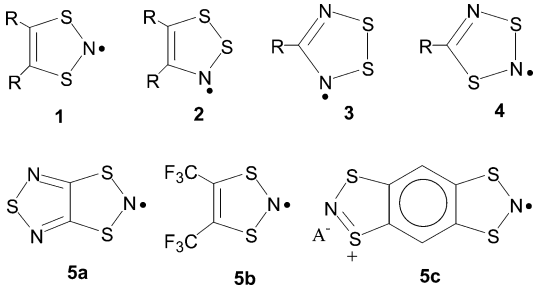

magnetic[5b,c] bistability around room temperature with a large hysteresis loop, whereas **5b** is a blue gas over a green paramagnetic liquid that exhibits magnetic hysteresis upon cooling and freezing, accompanied by a very large volume contraction.[6] Radical cation **5c** orders below 7.0 K ($A^- = GaCl_4^-$, γ phase)[7a] and 44 K ($A^- = FeCl_4^-$)[7b] as a ferromagnet and a ferrimagnet, respectively (Chart 1).

However, the major hindrance in utilizing thiazyl radicals as precursors to molecular magnets and conductors is their tendency to dimerize in the solid state via a bonding $\pi^*-\pi^*$ overlap of the constituent singly occupied molecular orbitals (SOMOs), leading to a diamagnetic singlet ground state. In solution, the dimerization energy of thiazyl radicals

Chart 2

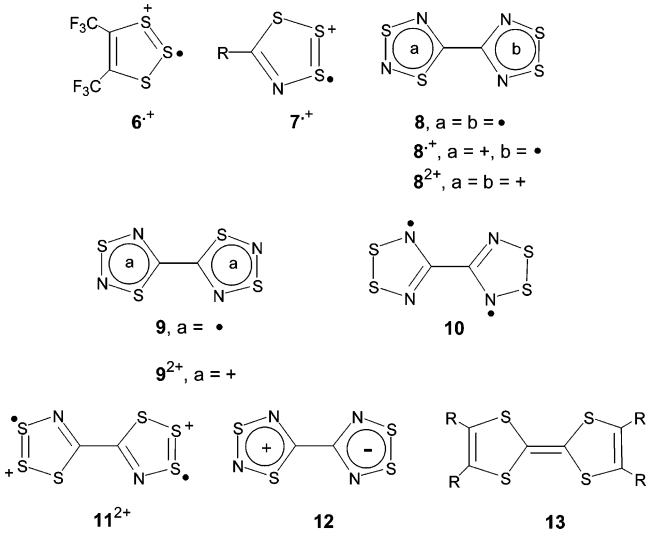

varies from ca. −35 kJ/mol for **3** (determined for PhCNSSN•)[31b] to 0 for **1** (determined for **5b**),[6a] and is very low for the paramagnetic liquid **4** (R = *t*-Bu[4b]). Among many characterized derivatives of **3**, only a small fraction was found to contain monomeric radical centers in the solid state.[1d,e,g,3] Room temperature paramagnetism has been demonstrated for salts containing both the −CNSSN•, and either the −CNSNS+ and −SNSSN+ moieties, dimerization of radical centers inhibited −CNSNS+ by the repulsion between the positively charged radical cations.[8] The AsF_6^- salts of radical cations $\mathbf{6}^{\bullet+}$ [9] and $\mathbf{7}^{\bullet+}$,[10,11] in which both the positive charge and an unpaired electron are incorporated into one heterocyclic ring, are also predominantly paramagnetic in the solid state, although some derivatives are found in a weakly associated state.[11] Thus, the thiazyl radical cations are likely to form undimerized or very weakly dimerized structures. Following this strategy, we pursued the preparation and characterization of $\mathbf{8}^{\bullet+}$ (Chart 2), in which the positive charge and an unpaired electron are separated onto different heterocyclic rings joined by a C−C single bond. This radical cation is one of the nine derivatives (given in Scheme 1 of ref 12a) formally obtainable from $\mathbf{9}^{2+}$ by reduction, isomerization, and reoxidation. $[CNSNS]_2[AsF_6]_2$, containing $\mathbf{9}^{2+}$, can be quantitatively prepared from the 2:1 cycloaddition reaction of $SNSAsF_6$ with cyanogen.[12] Double reduction of $\mathbf{9}^{2+}$ afforded the neutral diradical **9**, which possessed interesting physical properties but lacked full structural

(1) (a) Rawson, J. M.; Banister, A. J.; Lavender, I. *Adv. Heterocycl. Chem.* **1995**, *62*, 137. (b) Rawson, J. M.; McManus, G. D. *Coord. Chem. Rev.* **1999**, *189*, 135. (c) Oakley, R. T. *Adv. Mater*. **1994**, *6*, 798. (d) Rawson, J. M.; Palacio, F. *Struct. Bonding* **2001**, *100*, 93. (e) Rawson, J. M.; Alberola, A.; Whalley, A. *J. Mater. Chem.* **2006**, *16*, 2560. (f) Oakley, R. T. *Phosphorus, Sulfur Silicon Relat. Elem.* **2004**, *179*, 673. (g) Rawson, J. M.; Luzon, J.; Palacio, F. *Coord. Chem. Rev.* **2005**, *249*, 2631.

(2) (a) Makarov, A. Y.; Irtegova, I. G.; Vasilieva, N. V.; Bagryanskaya, I. Y.; Borrmann, T.; Gatilov, Y. V.; Lork, E.; Mews, R.; Stohrer, W.-D.; Zibarev, A. V. *Inorg. Chem.* **2005**, *44*, 7194. (b) Ikorskii, V. N.; Irtegova, I. G.; Lork, E.; Makarov, A. Yu.; Mews, R.; Ovcharenko, V. I.; Zibarev, A. V. *Eur. J. Inorg. Chem.* **2006**, *15*, 3061.

(3) (a) Alberola, A.; Less, R. J.; Pask, C. M.; Rawson, J. M.; Palacio, F.; Oliete, P.; Paulsen, C.; Yamaguchi, A.; Farley, R. D.; Murphy, D. M. *Angew. Chem. Int. Ed.* **2003**, *42*, 4782. (b) Banister, A. J.; Bricklebank, N.; Lavender, I.; Rawson, J. M.; Gregory, C. I.; Tanner, B. K.; Clegg, W.; Elsegood, M. R. J.; Palacio, F. *Angew. Chem., Int. Ed. Engl.* **1996**, *35*, 2533.

(4) (a) Burford, N.; Passmore, J.; Schriver, M. J. *J. Chem. Soc., Chem. Commun*. **1986**, 140. (b) Brooks, W. V. F.; Burford, N.; Passmore, J.; Schriver, M. J.; Sutcliffe, L. H. *J. Chem. Soc., Chem. Commun*. **1987**, 69. (c) Passmore, J.; Sun, X. *Inorg. Chem.* **1996**, *35*, 1313. (d) Burford, N.; Passmore, J.; Sun, X. *Phosphorus, Sulfur Silicon Relat. Elem.* **1994**, *93*−*94*, 487.

(5) (a) Matsuzaki, H.; Fujita, W.; Awaga, K.; Okamoto, H. *Phys. Rev. Lett.* **2003**, *91*, 017403. (b) Fujita, W.; Awaga, K. *Science* **1999**, *286*, 261. (c) McManus, G. D.; Rawson, J. M.; Feeder, N.; van Duijn, J.; McInnes, E. J. L.; Novoa, J. J.; Burriel, R.; Palacio, F.; Oliete, P. *J. Mater. Chem.* **2001**, *11*, 1992.

(6) (a) Awere, E. G.; Burford, N.; Mailer, C.; Passmore, J.; Schriver, M. J.; White, P. S.; Banister, A. J.; Oberhammer, H.; Sutcliffe, L. H. *J. Chem. Soc., Chem. Commun*. **1987**, 66. (b) Brownridge, S.; Haddon, R. C.; Oberhammer, H.; Parsons, S.; Passmore, J.; Schriver, M. J.; Sutcliffe, L.; Westwood, N. P. C. *J. Chem. Soc., Dalton Trans.* **2000**, 3365. (c) Du, H.; Haddon, R. C.; Krossing, I.; Passmore, J.; Rawson, J. M.; Schriver, M. J. *Chem. Commun*. **2002**, 1836.

(7) (a) Fujita, W.; Awaga, K. *Chem. Phys. Lett.* **2004**, *388*, 186. (b) Fujita, W.; Awaga, K.; Takahashi, M.; Takeda, M.; Yamazaki, T. *Chem. Phys. Lett.* **2002**, *362*, 97.

(8) (a) Bryan, C. D.; Cordes, A. W.; Fleming, R. M.; George, N. A.; Glarum, S. H.; Haddon, R. C.; MacKinnon, C. D.; Oakley, R. T.; Palstra, T. T. M.; Perel, A. S. *J. Am. Chem. Soc.* **1995**, *117*, 6880. (b) Britten, J. F.; Cordes, A. W.; Haddon, R. C.; Itkis, M. E.; Oakley, R. T.; Reed, R. W.; Robertson, C. M. *CrystEngComm*. **2002**, *4*, 205. (c) Banister, A. J.; Lavender, I.; Rawson, J. M.; Clegg, W.; Tanner, B. K.; Whitehead, R. J. *J. Chem. Soc., Dalton Trans.* **1993**, 1421.

(9) Cameron, T. S.; Haddon, R. C.; Mattar, S. M.; Parsons, S.; Passmore, J.; Ramirez, A. P. *J. Chem. Soc., Dalton Trans.* **1992**, 1563.

(10) (a) Boyle, P. D.; Parsons, S.; Passmore, J.; Wood, D. J. *J. Chem. Soc., Chem. Commun.* **1993**, 199. (b) Enright, G. D.; Morton, J. R.; Passmore, J.; Preston, K. F.; Thompson, R. C.; Wood, D. J. *Chem. Commun.* **1996**, 967. (c) Cameron, T. S.; Haddon, R. C.; Mattar, S. M.; Parsons, S.; Passmore, J.; Ramirez, A. P. *Inorg. Chem.* **1992**, *31*, 2274. (d) Decken, A.; Mattar, S. M.; Passmore, J.; Shuvaev, K. V.; Thompson, L. K. *Inorg. Chem.* **2006**, *45*, 3878.

(11) (a) Cameron, T. S.; Decken, A.; Kowalczyk, R. M.; McInnes, E. J. L.; Passmore, J.; Rawson, J. M.; Shuvaev, K. V.; Thompson, L. K. *Chem. Commun*. **2006**, 2277. (b) Decken, A.; Ebdah, M.; Kowalczyk, R. M.; Landee, C. P.; Passmore, J.; Shuvaev, K. V.; Thompson, L. K. *Inorg. Chem.* **2007**, in press.

(12) (a) Parsons, S.; Passmore, J.; White, P. S. *J. Chem. Soc., Dalton Trans.* **1993**, 1499. (b) Parsons, S.; Passmore, J.; Schriver, M. J.; White, P. S. *J. Chem. Soc., Chem. Commun.* **1991**, 369.

Scheme 1

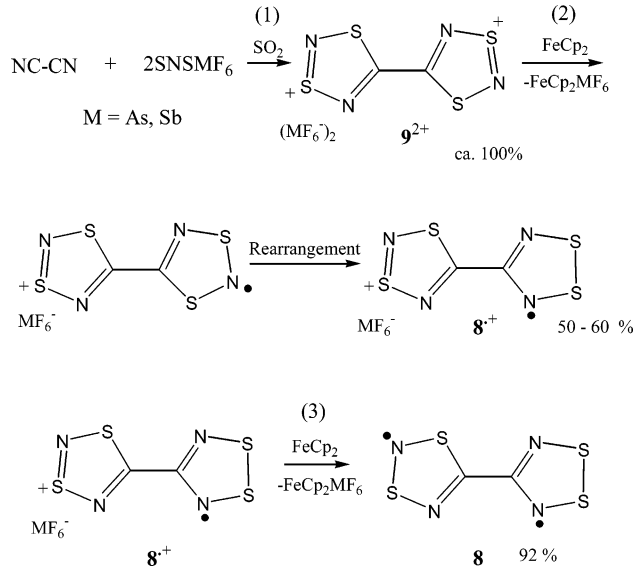

characterization.[13] The analogous isoelectronic **10**, which gave a conductor upon reaction with iodine, was prepared and fully characterized by Oakley and co-workers.[14] Recently, we demonstrated that it is also possible to prepare the mixed diradical **8**, which incorporates two isomeric 7π radical rings.[15] The family of diradicals, **8**,[15] **9**,[13] **10**,[14] and the isolobal $\mathbf{11}^{2+}$,[10a,b] are unique in that they contain two radical rings joined by a C−C single bond and do not adopt classical Lewis structures, for example **12** (Chart 2), but like O_2, have a thermodynamic preference for structures containing two unpaired electrons. We note that the extensively studied tetrathiafulvalene, TTF, **13**, and many related 14π bicycles adopt a closed-shell structure.

The focus of this article is the comprehensive study of the series $\mathbf{8}^{2+}$, $\mathbf{8}^{\bullet+}$, and **8** that present three oxidation states of the NSNSC−CNSSN framework. Of particular interest was radical cation $\mathbf{8}^{\bullet+}$ that could potentially form undimerized or weakly associated structures and exhibit interesting physical properties. Preliminary evidence has been presented for $\mathbf{8}^{\bullet+}$ [12] on the basis of IR spectroscopy and poor elemental analysis. Herein, we report an improved preparation of $\mathbf{8}^{\bullet+}$ in a pure state and its full characterization by X-ray, solid-state electron paramagnetic resonance (EPR), and magnetic susceptibility measurements.

A preliminary communication describing the preparation and solid-state structure of diradical **8** has been published.[15] A full account of the preparation and characterization of **8**, $\mathbf{8}MF_6$ (M = As, Sb), and $\mathbf{8}[AsF_6]_2$ is given below.

2. Experimental Section

2.1. Materials. Cyanogen $(CN)_2$,[16a] $SNSSbF_6$,[16b] $SNSAsF_6$,[16c] $\mathbf{9}[AsF_6]_2$,[12b] and AsF_5[16d] were prepared by previously published procedures. Ferrocene was obtained from Strem Chemicals and sublimed prior to use. Triphenylantimony (Fluka), and tetrabutylammonium chloride (Eastman Kodak, Lancaster Synthesis) were used as received. SO_2 (Liquid Air, 99.9998%) was distilled onto CaH_2 (Aldrich) and stored for at least 24 h. Acetonitrile (99.8%, anhydrous) was obtained from Aldrich and stored over CaH_2 (Aldrich) for at least 3 days.

2.2. General Procedures. All of the reactions were performed in two-bulb two-valve Pyrex vessels incorporating 50 mL bulbs in a closed system unless otherwise stated, using techniques that have been described previously.[16e] Solid reagents and crystals were manipulated and handled under a nitrogen atmosphere in a MBraun Unilab 1200/700 drybox.

Fourier transform infrared (FTIR) spectra of Nujol mulls between KBr disks were recorded on a Thermo Nicolet FTIR 470 spectrometer (32 scans, resolution 2.0 cm^{-1}). FT−Raman spectra were recorded at 293 K on a Bruker IFS66 FTIR equipped with a Bruker FRA106 FT−Raman accessory using a Nd:YAG laser (emission wavelength, 1064 nm; maximum laser power, 3009 mW; used laser power, 5.5%). Samples were sealed in melting-point capillaries, and data were collected in the backscattering mode (180° excitation; resolution 2.0 cm^{-1}).

Cyclic voltammetry measurements were carried out using a Pine Instrument Co. Bipotentiostat AFBPC1 on dilute solutions of analyte in doubly distilled (P_2O_5/CaH_2) degassed acetonitrile at 25 °C ($\mathbf{8}^{\bullet+}$ and $\mathbf{8}^{2+}$) and 44 °C ($\mathbf{9}^{2+}$), with 0.1 M n-Bu_4NPF_6 supporting electrolyte in a single-compartment cell fitted with three platinum wires, referenced to the ferrocene/ferrocenium couple at 0.38 V versus the saturated calomel electrode (SCE).[29a]

Electron paramagnetic resonance (EPR) spectra of **8** were recorded with modified Varian E3 and E104 spectrometers. Microwave frequencies were measured with an EIP 371 frequency counter, and the magnetic field was calibrated with a solid sample of 2,2-diphenyl-1-picrylhydrazyl (DPPH) ($g = 2.0036$) and a Bell 640 Gaussmeter. Both solution and solid-state EPR spectra of $\mathbf{8}SbF_6$ were recorded with a MiniScope MS200 spectrometer, and the g factors were determined by comparison with the external solid DPPH standard.

Variable-temperature magnetic susceptibility data were obtained using a Quantum Design MPMS5S Squid magnetometer that employed a magnetic field of 1000 Oe. The compounds were contained in polycarbonate capsules. Background corrections for the sample holders and diamagnetism (Pascal's constants) were applied.

Mass spectra (20 eV, EI) were measured on a Kratos MS50TC spectrometer. The samples were contained in sealed melting-point tubes at atmospheric pressure. They were opened and rapidly introduced via the direct-inlet method by maintaining a temperature of 250 °C.

Chemical analysis of $\mathbf{8}AsF_6$ was carried out by the Laboratory of Microanalysis, Novosibirsk Institute of Organic Chemistry, Russia. The other chemical analyses were obtained from Galbraith Laboratories. Inc., Knoxville, TN.

2.3. Computational Methods. Molecular geometries, vibrational frequencies, and NBO charges of all of the molecules and molecular

(13) Antorrena, G.; Brownridge, S.; Cameron, T. S.; Palacio, F.; Parsons, S.; Passmore, J.; Thompson, L. K.; Zarlaida, F. *Can. J. Chem.* **2002**, *80*, 1568.

(14) (a) Bryan, C. D.; Cordes, A. W.; Haddon, R. C.; Hicks, R. G.; Oakley, R. T.; Palstra, T. T. M.; Perel, A. J. *J. Chem. Soc., Chem. Commun.* **1994**, 1447. (b) Bryan, C. D.; Cordes, A. W.; Goddard, J. D.; Haddon, R. C.; Hicks, R. G.; MacKinnon, C. D.; Mawhinney, R. C.; Oakley, R. T.; Palstra, T. T. M.; Perel, A. J. *J. Am. Chem. Soc.* **1996**, *118*, 330.

(15) Cameron, T. S.; Lemaire, M. T.; Passmore, J.; Rawson, J. M.; Shuvaev, K. V.; Thompson, L. K. *Inorg. Chem.* **2005**, *44*, 2576.

(16) (a) Brauer, G. *Handbook of preparative inorganic chemistry*; 2nd ed.; Academic Press: New York, 1963; p 663. (b) Passmore, J.; Shuvaev, K. V.; Mailman, A.; Cameron, T. S. *Inorg. Chem.* **2005**, *44*, 6524. (c) Awere, E. G.; Passmore, J. *J. Chem. Soc., Dalton Trans.* **1992**, 1343. (d) Aris, D. R.; Knapp, C.; Passmore, J.; Wang, X. *J. Fluorine Chem.* **2005**, *126*, 1368. (e) Murchie, M. P.; Kapoor, R.; Passmore, J.; Schatte, G. *Inorg. Synth.* **1996**, *31*, 80.

aggregates were calculated at the MPW1PW91[17a] level of theory employing the 6-31G* and 6-311G+(2df) basis sets as implemented into *Gaussian03W* suite of programs.[17b] Spin densities and hyperfine coupling constants were computed at the MPW1PW91 level using the EPR-III basis set[18a] for C and N atoms and the TZVP basis set[18b,c] for S atoms. The singlet−triplet gaps of **8**−**10** were calculated using the CASPT2(8,8) method[19a,b] on the geometries optimized with the CASSCF(8,8)[19c−e] method using the *MOLPRO* program.[20] The TZVPP basis set was used as implemented in the *MOLPRO* internal basis set library.

Open-shell singlet and triplet states of **8**, isolated molecules $\mathbf{8}^{\bullet+}$ and $\mathbf{8}^{2+}$, dimeric conformations of $[\mathbf{8}^{\bullet+}]_2$ and $[\mathbf{8}]_2$ were fully optimized into minima [MPW1PW91/6-31G*], as indicated by the absence of imaginary frequencies. Single-point energy calculations of paramagnetic excited states of dimers were performed using fully optimized [MPW1PW91/6-31G*] closed-shell singlet geometries as inputs. The natural orbital populations were computed using the CASSCF(6,6)/6-31G* method as implemented into the *Gaussian03W* suite of programs.[17b] Vibrational frequencies were animated and assigned using *ChemCraft*.[21]

2.4. Syntheses. 2.4.1. Preparation of $9[SbF_6]_2$. CAUTION! *Manipulations with very poisonous cyanogen should be carried out in a very efficient fume hood with a good vacuum line; a closed system with SO_2 is potentially explosive when heated to 40*−*50 °C; hence, all of the glassware has to be well made and tested to withstand pressures of 3*−*5 atm before performing this experiment.*

$(CN)_2$ (0.613 g, 11.8 mmol) was condensed into one bulb of a two-bulb vessel and dissolved in 32.83 g of SO_2. The solution was quantitatively transferred into the second bulb containing S_2NSbF_6 (7.25 g, 23.1 mmol), and the mixture was gently heated at 45 °C for 3 days, with the valve to the second bulb was kept in a closed position to prevent evaporation of the solvent into the cooler parts of the vessel. After 3 days, a yellow-brown solution over a colorless polycrystalline product $\mathbf{9}[SbF_6]_2$ (4.10 g) was separated from the yellow-brown soluble product. This solution was evaporated, and the resultant residue further recrystallized from SO_2, affording an additional amount of 2.98 g of highly crystalline, colorless, pure $\mathbf{9}[SbF_6]_2$ (overall yield 88% based on eq 1, Scheme 1, using S_2NSbF_6 as a limiting reagent). Raman frequencies, cm^{-1} (relative intensity is given in brackets): 1499(95), 1215(11), 952(17), 902(8), 795(73), 683(10), 646(71) [$\nu_1SbF_6^-$], 590(48), 573(6) [$\nu_2SbF_6^-$], 561(3) [$\nu_2SbF_6^-$], 355(19), 292(23), 283(23) [$\nu_5SbF_6^-$], 257(12). All of the vibrational frequencies are assigned to $\mathbf{9}^{2+}$ [13] and the SbF_6^- anion.[22,16b]

2.4.2. Preparation of $8AsF_6$ Via Reduction of $9[AsF_6]_2$ by a Mixture of $SbPh_3$ and NBu_4Cl. In a typical experiment, $\mathbf{9}[AsF_6]_2$ (2.02 g, 3.45 mmol) and a mixture of $SbPh_3$ (0.611 g, 1.73 mmol) and NBu_4Cl (0.958 g, 3.45 mmol) were placed into separate bulbs of a two-bulb vessel, and SO_2 (ca. 15 mL) was condensed into each bulb. The reducing agent was added to the solution of $\mathbf{9}[AsF_6]_2$ in 3 mL portions over 3 days with rigorous stirring while sonicating the reaction mixture every 6−8 h. After 3 days, the mixture turned from a yellow to a black solution over a black insoluble solid. The solid was washed five times with 10 mL portions of SO_2 to afford 0.750 g of crude, black $\mathbf{8}AsF_6$. This solid was further purified by dissolution in degassed, dry MeCN and filtered through a fine frit to separate it from impurities of **9**, which are insoluble in MeCN. Finally, the solution was evaporated, and the black solid was washed three times with a small amount of SO_2 to yield pure $\mathbf{8}AsF_6$ (0.612 g, 44% based on eq 2, Scheme 1, using $\mathbf{9}[AsF_6]_2$ as a limiting reagent) as a black-violet powder. Elem Anal. for $C_2S_4N_4AsF_6$, Found/Calcd: C, 6.04/6.05; N, 14.00/14.10; S, 32.42/32.29; F, 28.51/28.70. IR frequencies with assignments are listed in Table 1.

2.4.3. Preparation of $8AsF_6$ Using Ferrocene as a Reducing Agent. The reaction was carried out analogously to that when using a mixture of $SbPh_3$ and NBu_4Cl in Section 2.4.2. Amounts of reagents: $\mathbf{9}[AsF_6]_2$ (2.33 g, 3.98 mmol), $FeCp_2$ (0.740 g, 3.98 mmol). The recovered quantity of $\mathbf{8}AsF_6$ was 0.910 g (56% based on eq 2, Scheme 1, using ferrocene as a limiting reagent).

2.4.4. Preparation of $8SbF_6$. The reaction was carried out analogously to that described for $\mathbf{8}AsF_6$ in Section 2.4.3. Amounts of reagents: $\mathbf{9}[SbF_6]_2$ (3.31 g, 4.87 mmol), $FeCp_2$ (0.851 g, 4.58 mmol). The recovered quantity of $\mathbf{8}SbF_6$ was 1.292 g (60% based on eq 2, Scheme 1, using ferrocene as a limiting reagent). IR, cm^{-1}: 1343 (w), 1296 (m), 1232 (vw), 1109 (w), 1093 (mw), 948 (w), 903 (w), 822 (ms), 790 (m), 769 (m), 661 (vs) [$\nu_3SbF_6^-$], 653 (vs), 644 (vs) [$\nu_1SbF_6^-$], 593 (vw), 580 [$\nu_2SbF_6^-$], 564 [$\nu_2SbF_6^-$], 508 (m), 442 (m), 425 (vw). All of the vibrational frequencies are assigned to $\mathbf{8}^{\bullet+}$ (Table 1) and the SbF_6^- anion.[22,16b] Suitable crystals of $\mathbf{8}SbF_6$ were grown at room temperature from a saturated SO_2 solution. An EPR spectrum of a green solution of $\mathbf{8}SbF_6$ in SO_2 is depicted in Figure 9.

2.4.5. Preparation of $8[AsF_6]_2$ by Oxidation of $8AsF_6$ with AsF_5. CAUTION! *Utmost care must be taken when performing operations with very toxic arsenic pentafluoride*. SO_2 (4.59 g) was condensed onto $\mathbf{8}AsF_6$ (0.970 g, 2.44 mmol), followed by the addition of AsF_5 (0.650 g, 3.82 mmol). The mixture was slowly warmed up and stirred for 1 day, producing a yellow-brown solution over a yellow-brown solid. The residue was multiply recrystallized from SO_2 to yield pure $\mathbf{8}[AsF_6]_2$, 1.136 g (80% using $\mathbf{8}AsF_6$ as a limiting reagent). Elem Anal. for $C_2S_4N_4As_2F_{12}$, Found/Calcd: C,

(17) (a) Adamo, C.; Barone, V. *J. Chem. Phys.* **1998**, *108*, 664. (b) Frisch, M. J.; Trucks, G. W.; Schlegel, H. B.; Scuseria, G. E.; Robb, M. A.; Cheeseman, J. R.; Montgomery, J. A., Jr.; Vreven, T.; Kudin, K. N.; Burant, J. C.; Millam, J. M.; Iyengar, S. S.; Tomasi, J.; Barone, V.; Mennucci, B.; Cossi, M.; Scalmani, G.; Rega, N.; Petersson, G. A.; Nakatsuji, H.; Hada, M.; Ehara, M.; Toyota, K.; Fukuda, R.; Hasegawa, J.; Ishida, M.; Nakajima, T.; Honda, Y.; Kitao, O.; Nakai, H.; Klene, M.; Li, X.; Knox, J. E.; Hratchian, H. P.; Cross, J. B.; Bakken, V.; Adamo, C.; Jaramillo, J.; Gomperts, R.; Stratmann, R. E.; Yazyev, O.; Austin, A. J.; Cammi, R.; Pomelli, C.; Ochterski, J. W.; Ayala, P. Y.; Morokuma, K.; Voth, G. A.; Salvador, P.; Dannenberg, J. J.; Zakrzewski, V. G.; Dapprich, S.; Daniels, A. D.; Strain, M. C.; Farkas, O.; Malick, D. K.; Rabuck, A. D.; Raghavachari, K.; Foresman, J. B.; Ortiz, J. V.; Cui, Q.; Baboul, A. G.; Clifford, S.; Cioslowski, J.; Stefanov, B. B.; Liu, G.; Liashenko, A.; Piskorz, P.; Komaromi, I.; Martin, R. L.; Fox, D. J.; Keith, T.; Al-Laham, M. A.; Peng, C. Y.; Nanayakkara, A.; Challacombe, M.; Gill, P. M. W.; Johnson, B.; Chen, W.; Wong, M. W.; Gonzalez, C.; Pople, J. A. *Gaussian 03*, revision C.02; Gaussian, Inc.: Wallingford, CT, 2004.

(18) (a) *Recent Advances in Density functional Methods*; Chong, D. P., Ed.; World Scientific: Singapore, 1995; Part I. (b) Schaefer, A.; Horn, H.; Ahlrichs, R. *J. Chem. Phys.* **1992**, *97*, 2571. (c) Schaefer, A.; Huber, C.; Ahlrichs, R. *J. Chem. Phys.* **1994**, *100*, 5829.

(19) (a) Werner, H.-J. *Mol. Phys.* **1996**, *89*, 645. (b) Celani, P.; Werner, H.-J. *J. Chem. Phys.* **2000**, *112*, 5546. (c) Werner, H.-J.; Knowles, P. J. *J. Chem. Phys.* **1985**, *82*, 5053. (d) Knowles, P. J.; Werner, H.-J. *Chem. Phys. Lett.* **1985**, *115*, 259. (e) Busch, T.; Degli Esposti, A.; Werner, H.-J. *J. Chem. Phys.* **1991**, *94*, 6708.

(20) Amos, R. D.; Bernhardsson, A.; Berning, A.; Celani, P.; Cooper, D. L.; Deegan, M. J. O.; Dobbyn, A. J.; Eckert, F.; Hampel, C.; Hetzer, G.; Knowles, P. J.; Korona, T.; Lindh, R.; Lloyd, A. W.; McNicholas, S. J.; Manby, F. R.; Meyer, W.; Mura, M. E.; Nicklass, A.; Palmieri, P.; Pitzer, R.; Rauhut, G.; Schutz, M.; Schumann, U.; Stoll, H.; Stone, A. J.; Tarroni, R.; Thorsteinsson, T.; Werner, H.-J. *MOLPRO 2002.6 a package of ab initio programs*; MOLPRO 2002.6: Birmingham, UK, 2003.

(21) Zhurko, D. A.; Zhurko, G. A. *ChemCraft 1.5*. http://www.chemcraftprog.com/.

(22) (a) Nakamoto, K. *Infrared and Raman Spectra of Inorganic and Coordination Compounds*; Wiley: New York, 1986. (b) A minor splitting (ca. 10 cm^{-1}) of the ν_2 frequency (E_g) of the SbF_6^- anion is consistent with a slight distortion from an ideal O_h symmetry.

Table 1. Experimental and Calculated [MPW1PW91/6-311+(2df)] Vibrational Frequencies of **8**$[AsF_6]_2$, **8**AsF_6, and **8** (Atom Labeling is Given in Figure 1)

8$[AsF_6]_2$			**8**AsF_6			**8**			
IR	Raman	calcd $\mathbf{8}^{2+}$ (IR, Raman)	IR	Raman[a]	calcd $\mathbf{8}^{\cdot+}$ (IR, Raman)	IR	Raman	calcd **8** (IR, Raman)	assignment[b]
		41(0, 0)			60 (0, 0)			42 (0, <1)	oop ring twist
		104 (2, 0)			93 (1, 0)			96 (<1, 0)	oop ring folding
		108 (1, <1)			99 (1, 130)			111 (1, 1)	ip ring twist
		278 (<1, 3)			282 (6, 350)			277 (0, 1)	ring breathe
		291 (4, 4)			277 (4, <1)			257 (0, <1)	oop ring deform.
	298w	368 (2, 5)			369 (8, 46)		282w	355 (3, 10)	ip ring twist
		413 (<1, 0)			289 (2, 0)			283 (<1, 3)	$\delta(N_3S_3S_4N_4)$ oop
	374mw		369w						$\nu_5(AsF_6^-)$[c]
			398 m						$\nu_4(AsF_6^-)$
	490 m	422 (1, 29)	426vw		402 (8, 1000)	420sh	418mw	405 (1, 30)	$\nu(S_3\text{-}S_4)$
444 m		459 (15, 0)	442 m		444 (12, 1)			182 (9, 1)	$\delta(S_2N_2S_1)$ oop
550 m	553w	573 (11, 10)	508 m		524 (13, 2)	501 m		522 (6, 9)	(−CNSSN) ring twist
574 m			579w						$\nu_2(AsF_6^-)$
561 m		597 (9, 1)	549mw		564 (14, <1)	520 m		540 (12, <1)	$\delta(N_1C_1C_2)$ oop
589 m	590w	602 (13, 11)	593vw		599 (6, 2300)	544mw	551vw	543 (3, 5)	$\delta_{as}(S_2N_2S_1)$ ip
coalesAsF_6^-	682 m	669 (8, 2)	654s		667 (5, 58)	667vw		641 (1, 4)	$N(C_1\text{-}S_2)$
coalesAsF_6^-			646s						$\nu_1(AsF_6^-)$
666s	671w		666s			675vw[e]			$\nu_3(AsF_6^-)$
700s	692vw	772 (4, 4)			728 (1, 2)	648vw		731 (4, 7)	$\delta(C_1\text{-}C_2)$ oop
778 m	779w	777 (9, 15)	768 m		780 (94, 2800)	696vs	698s	702 (11, 23)	$\delta_{as}(N_3C_2N_4) + \delta_{as}(N_2S_1N_1)$ ip
829 m	830 m	844 (27, 25)	821ms		844 (34, 612)	769s	772w	819 (34, 15)	$\delta_s(N_3C_2N_4) + \delta_s(N_2S_1N_1)$ ip
863 m	864vw	870 (23, 2)	not obsvd		851 (84, 1250)	738s	719s	759 (30, 147)	$\nu(S_1\text{-}N_1)$
881ms		905 (5, 1)	790 m		811 (170, 30^3)	808s	805w	827 (22, 8)	$\delta_s(N_3S_3S_4N_4)$ ip
975 m	975vw	973 (62, 4)	902mw		911 (8, 402)	875mw	877vw	893 (3, 53)	$\delta_{as}(N_3S_3S_4N_4)$ ip
934 m	935vw	1013 (16, 9)	947w		972 (4, 1313)	839vw	836w	847 (41, 57)	$\nu(S_2\text{-}N_2)$
1152mw		1167 (27, 9)	1108w		1141 (2, 3210)	1076s	1082w	1134 (28, 12)	$\nu(C_1\text{-}C_2)$[d]
1276 m		1322 (11, 9)	1298 m		1334 (123, 10^3)	1342vw		1312 (7, 56)	$\nu(C_2\text{-}N_4)$
1362s	1361vw	1419 (64, 104)	1342 w		1430 (24, 10^3)	1318w	1315w	1410 (118, 482)	$\nu(C_2\text{-}N_3)$
1490sh	1494s	1553 (4, 403)	1472 m		1558 (3, 10^3)	1500w	1502s	1617 (39, 10^3)	$\nu(C_1\text{-}N_1)$
1120ms[e]	1120vw[e]		977vw,1092mw[e]			1047w[e]			

[a] Not obtained because of interfering fluorescence scattering. [b] Visualization of the vibrations was performed using *ChemCraft* (ref 21). The major components of the vibrational modes are given but in fact are often much more complex than indicated. [c] Distortion of the AsF_6^- anions from O_h to C_1 symmetry (Figure S2 in the Supporting Information) makes all of the vibrational frequencies IR and Raman active. [d] This stretching frequency was heavily mixed with $\nu(C_2-N_4)$, $\nu(C_2-N_3)$, and $\nu(C_1-N_1)$ modes (the graphical representation is given in Figure S6 in the Supporting Information). [e] Unassigned but general features of vibrational spectra of **8**$[AsF_6]_2$, **8**AsF_6, and **8**. These features are also observed in the vibrational spectra of **9** and $\mathbf{9}^{2+}$ (ref 13).

4.15/4.10; N, 9.52/9.56. IR and Raman frequencies with assignments are listed in Table 1.

2.4.6. Preparation of 8. In a typical experiment, **8**AsF_6 (0.72 g, 1.8 mmol) was stirred with $FeCp_2$ (0.37 g, 2.0 mmol) in SO_2 (ca. 20 mL) in the dark for 2 days. The insoluble gray precipitate **8** was filtered and washed with SO_2 to yield 0.350 g of product (92% using **8**AsF_6 as a limiting reagent). Elem Anal. for $C_2S_4N_4$, Found/Calcd: C, 11.52/11.53; N, 25.81/26.90. Mass spectrum (20 eV, EI): 208 (100%, $[C_2S_4N_4]^+$), 162 (19%, $[C_2S_3N_3]^+$), 144 (18%, $[C_2S_2N_4]^+$), 130 (80%, $[C_2S_2N_3]^+$), 116 (3%, $[C_2S_2N_2]^+$), 104 (1%, $[C_2S_4N_4]^{2+}$), 78 (52%, S_2N^+), 64 (4%, S_2^+), 46 (7%, NS^+).

Crystals of **8** were grown by vacuum-gradient sublimation (10^{-3} Torr), using an oven of 76 cm in length, with a temperature gradient 110−80−50 °C.

IR and Raman frequencies with assignments of the products are listed in Table 1. Actual IR and Raman spectra of the products are included in Figures S10−S15 in the Supporting Information.

2.5. In Situ EPR Study of Rearrangement of 8. A vessel incorporating a quartz tube (o.d. = 4 mm, i.d. = 2 mm) and one thick-walled 25 mL round-bottom flask coated with aluminum foil was loaded with **8**AsF_6 (0.397 g, 1.00 mmol), $SbPh_3$ (0.177 g, 0.50 mmol), and NBu_4Cl (0.278 g, 1.00 mmol), followed by the addition of 14.6 g of SO_2. The reaction mixture was rigorously stirred for 1 min and quickly filtered into the quartz tube, after which a series of EPR spectra were immediately recorded (Figure 11).

2.6. X-ray Crystal Structure Determination. The measurements were made on a Rigaku AFC5R diffractometer (compound **8**) or a Bruker AXS P4/SMART 1000 diffractometer (compounds **8**SbF_6 and **8**$[AsF_6]_2$). The crystal of **8**SbF_6 was twinned (multicomponent), and the orientation matrix for the major component was determined.[23a] The structures were solved by direct methods[23b] and all of the atoms were refined anisotropically.

3. Results and Discussion

3.1. Preparation of 8MF_6 (M = As, Sb), 8$[AsF_6]_2$, and 8. To prepare **8**MF_6, we followed the methodology previously described in ref 12a with some modifications in the reaction conditions. In the previous work, the reagents were mixed together directly. In the present work, we found that the kinetic conditions that minimize the formation of byproducts are critical for the successful isolation of pure **8**MF_6 (M = As, Sb) in high yield. This was achieved by the step-by-step addition of an SO_2 solution of $FeCp_2$ to an SO_2 solution of **9**$[MF_6]_2$ (eq 2, Scheme 1), thus ensuring the presence of an excess of dication $\mathbf{9}^{2+}$ during the reduction process. This procedure does not entirely exclude the formation of the

(23) (a) RLATT 2.72, Bruker AXS, Inc.: Madison, WI, 1999 (b) Sheldrick, G.M. *SHELX97*, University of Göttingen: Göttingen, Germany, 1997.

Scheme 2

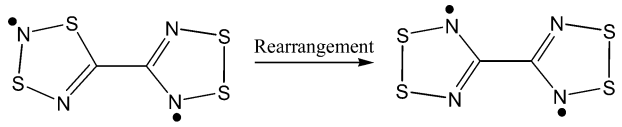

8 **10**

double reduction byproducts **8** and **9**; however, it increases the yield of **8**MF_6 (M = As, Sb) and makes its purification easier. After washing off the very soluble $FeCp_2MF_6$, the crude residue left from the reduction consists of **8**MF_6 and the doubly reduced species **8** and **9**. The latter are insoluble in MeCN; therefore, **8**MF_6 can be extracted by dissolution of the mixture in acetonitrile and filtering it through a fine frit, followed by evaporating MeCN from the filtrate and washing the residue with SO_2. The above described procedure appears to be the best for isolation of analytically pure **8**MF_6 (M = As, Sb) in 50−60% yields.

8AsF_6 was further reoxidized with AsF_5 to afford the mixed dication salt **8**$[AsF_6]_2$, isolated as an analytically pure colorless solid in 80% yield.

Reduction of **8**MF_6 (M = As, Sb) with ferrocene afforded analytically pure **8** in high yield (Scheme 1, eq 3). Formation of **8** is perhaps surprising given the strong tendency of RCNSNS• radicals to rearrange rapidly to the more-stable RCNSSN• in solution[4,8c] and in some cases upon heating in the solid state.[24] In solution, **8** also rearranged to **10** (Scheme 2), as evidenced by in situ EPR studies (Section 3.5.2.); however, because the diradical is extremely insoluble in SO_2, it precipitated out of the solution before significant rearrangement took place. Because of this fortunate circumstance, **8** presents the kinetic product isolated as an analytically pure solid from SO_2, whereas the formation of the thermodynamically preferred **10** is inhibited. In fact, no vibrational bands attributable to **10**[14a] were detected in the IR spectrum of **8** (Table 1), indicating that the amount of the symmetric isomer, if present, was negligible. Detection of **10** in a SO_2 solution by EPR is only possible due to the great sensitivity of this technique (down to a 10^{-7} M concentration of radical species can be detected). To prove this point further (negligible contribution of the rearrangement route), we performed a test experiment in which a suspension of **8** in MeCN was stirred for 2 days in room light. Under these conditions, if the rearrangement reaction of **8** into **10** was significant; the IR spectrum of the residue would indicate a mixture of either both isomers or only **10**. However, the IR spectrum recorded at the end of the experiment indicated no change in composition of the starting materials; that is, no bands were attributable to **10**.[25] Therefore, the extremely low solubility of **8** in both SO_2 and MeCN thwarts the thermodynamically favorable rearrangement (Scheme 2) and allows the mixed diradical to be successfully isolated as an analytically pure, stable solid.

The instability of the −CNSNS• ring with respect to its symmetric isomer has been a serious impediment in the experimental exploration of the family of 7π RCNSNS• radicals[4,8c,24] and their exploitation as molecular magnetic materials. Notably, up to now only five derivatives of this rare class of thiazyl radicals have been isolated in the solid state with only three characterized by magnetic susceptibility measurements,[13,24] including the mixed diradical **8** (all diamagnetic). On the other hand, more than 40 derivatives of the isomeric RCNSSN• are known, owing to its thermodynamic stability and accessibility via several preparative routes including the rearrangement of RCNSNS•.[4] In this light, characterization of a new derivative of the RCNSNS• ring system as a moiety of diradical **8** is especially significant.

3.2. Crystal Structures. Crystallographic data for all of the compounds are compiled in Table 3. The experimental and calculated internal parameters of $\mathbf{8}^{2+}$, $\mathbf{8}^{\bullet+}$, and **8** are given in Table 2. For consistency, the numbering scheme used in **8** was also adopted for $\mathbf{8}^{\bullet+}$ and $\mathbf{8}^{2+}$. Below, we present an analysis of each solid-state structure in turn.

3.2.1. Crystal Structure of 8. The experimental internal parameters of the −CNSSN• and −CNSNS• radical halves of **8** (Table 2) are similar to those found for **10**[14] and $C_6H_4(CNSNS)_2$.[24]

Figure 1 illustrates the $\pi^*-\pi^*$ dimer of **8**, with two molecules displaced about an inversion center, such as to allow $\pi^*-\pi^*$ interactions between different isomeric rings. Diradical **10** forms a similar cofacial $\pi^*-\pi^*$ dimer despite the electrostatic repulsion between like atoms.[14] In $[\mathbf{8}]_2$, the electrostatic repulsion is decreased by four electrostatically favorable $S^{\delta+}\cdots N^{\delta-}$ interactions (NBO charges listed in Table 5). Density functional theory (DFT) calculations in the gas phase gave the lowest-energy dimer with a geometry the same as that observed in the X-ray structure (computational Section 3.7.3.). The intradimeric S···S and S···N distances observed in $[\mathbf{8}]_2$ are similar to those of other thiazyl radical dimers,[1] falling in the range of 2.9−3.1 Å. These distances are less than the sum of the anisotropic van der Waals radii perpendicular to the bonding plane for S···S (4.06 Å) and S···N (3.49 Å) interactions,[26] implying an efficient bonding overlap of SOMOs and, consequently, the diamagnetic singlet ground state. Dimerization of **8** also causes a slight bending of the molecules, with a dihedral angle of 5.4° between the least-square planes of the −CNSSN• and −CNSNS• rings. The C(1)−C(2) bond distance of **8** [1.491(9) Å] is only slightly longer than the standard value of the single sp^2-sp^2 C−C bond length (1.46 Å)[27b] and is close to that of $H_5C_6-C_6H_5$ [1.493(3) Å],[27a] implying that the two heterocyclic rings are relatively independent of one another; that is, the diradical is almost disjoint in nature (a more-detailed description of the electronic structure of **8** is given in Section 3.7.1.).

It is noteworthy that **8** and **10** are essentially isomorphous (monoclinic; space groups $P2_1/n$ and $P2_1/c$, respectively; mutually transposable; Figure S1 in the Supporting Informa-

(24) Banister, A. J.; Rawson, J. M.; Clegg, W.; Birkby, S. L. *J. Chem. Soc., Dalton. Trans.* **1991**, 1099.
(25) The major vibrational bands in the IR spectrum of **10** are (cm^{-1}): 1244, 804, 793, 784, and 507, as taken from ref 14a.
(26) Nyburg, S. C.; Faerman, C. H. *Acta. Crystallogr.* **1985**, *B41*, 274.
(27) (a) Charbonneau, G.-P.; Delugeard, Y. *Acta Crystallogr., Sect. B* **1977**, *33*, 1586. (b) Gleiter, R. *Angew. Chem., Int. Ed. Engl.* **1981**, *20*, 444.

Table 2. Calculated[a] and Experimental (X-ray) Bond Distances and Angles of Monomeric $\mathbf{8}^{2+}$, $\mathbf{8}^{\bullet+}$, and **8**

	$\mathbf{8}^{2+}$		$\mathbf{8}^{\bullet+}$		**8**				
	X-ray	calcd MPW	X-ray	calcd MPW	X-ray	triplet MPW	closed-shell singlet, MPW	triplet CAS	singlet[b] CAS
					Bond distances (Å)				
C_1-C_2	1.450(12)[b]	1.476	1.460(26)[c]	1.459	1.491(9)	1.466	1.456	1.487	1.485
C_1-N_1	1.309(11)	1.296	1.342(26)	1.297	1.286(9)	1.278	1.281	1.245	1.246
N_1-S_1	1.609(7)	1.610	1.579(15)	1.609	1.668(5)	1.643	1.640	1.666	1.667
S_1-N_2	1.604(7)	1.585	1.597(16)	1.585	1.649(6)	1.643	1.623	1.647	1.648
N_2-S_2	1.578(7)	1.589	1.602(16)	1.602	1.648(6)	1.653	1.622	1.650	1.648
S_2-C_1	1.725(9)	1.747	1.706(19)	1.744	1.718(7)	1.770	1.748	1.775	1.772
C_2-N_3	1.319(12)	1.330	1.307(23)	1.313	1.341(8)	1.325	1.307	1.322	1.322
N_3-S_3	1.562(8)	1.568	1.612(17)	1.614	1.634(5)	1.621	1.639	1.626	1.626
S_3-S_4	2.029(3)	2.068	2.108(8)	2.124	2.098(3)	2.119	2.144	2.128	2.129
S_4-N_4	1.573(8)	1.574	1.637(16)	1.624	1.638(6)	1.623	1.657	1.630	1.631
C_2-N_4	1.341(11)	1.330	1.360(26)	1.330	1.338(8)	1.328	1.330	1.318	1.318
					Bond angles (deg)				
$C_1-N_1-S_1$	111.8(6)	113.2	111.2(12)	112.6	111.4(5)	113.2	112.0	114.1	114.0
$N_1-S_1-N_2$	103.0(4)	101.7	104.2(8)	102.8	102.3(3)	102.8	102.6	101.0	100.9
$S_1-N_2-S_2$	112.5(4)	114.7	112.1(9)	113.4	110.7(3)	111.3	112.3	112.3	112.4
$N_2-S_2-C_1$	97.4(4)	95.4	96.9(8)	95.8	97.1(3)	96.1	95.9	95.4	95.4
$S_2-C_1-N_1$	115.3(7)	115.1	115.5(13)	115.3	118.4(5)	116.7	117.2	117.2	117.3
$N_1-C_1-C_2$	124.0(8)	122.2	123.7(16)	126.9	123.4(6)	124.1	129.4	123.7	123.9
$S_2-C_1-C_2$	120.7(7)	122.8	120.7(13)	117.8	118.0(5)	119.2	113.4	119.1	118.7
$C_1-C_2-N_3$	122.2(9)	120.6	121.8(16)	120.6	121.1(6)	120.3	121.0	119.5	119.5
$C_1-C_2-N_4$	117.5(8)	119.7	113.3(15)	114.7	114.0(6)	116.4	112.3	116.9	116.8
$C_2-N_3-S_3$	115.2(7)	115.7	113.7(13)	113.8	111.9(5)	114.3	113.2	114.4	114.4
$N_3-S_3-S_4$	95.2(3)	94.5	95.0(6)	94.3	95.7(2)	94.2	94.2	93.9	93.9
$S_3-S_4-N_4$	95.0(3)	94.0	94.1(6)	93.4	93.9(2)	93.5	93.1	93.1	93.1
$S_4-N_4-C_2$	114.3(6)	116.0	112.3(12)	113.7	113.3(4)	114.7	112.8	115.0	114.9
$N_4-C_2-N_3$	120.2(8)	119.8	124.9(16)	124.8	124.9(6)	123.3	126.6	123.6	123.7
					Selected dihedral angles (deg)				
$S_2-C_1-C_2-N_4$	3(1)	0	7(2)	0	4.1(8)	0	0	0	0

[a] MPW stands for MPW1PW91/6-311+G(2df), and CAS stands for CASSCF(8,8)/TZVPP. The atom labeling scheme is given in Figure 1. [b] The CAS calculation is a multireference calculation, which is always open shell because the orbital occupations have not been restricted. [c] Slightly shorter than the sp^2-sp^2 C−C bond length observed in biphenyl $H_5C_6-C_6H_5$ [1.493(3) Å, ref 27a]. The standard value of the single sp^2-sp^2 C−C bond length equals 1.46 Å (ref 27b).

Table 3. Crystallographic Data for $\mathbf{8}[AsF_6]_2$, $\mathbf{8}SbF_6$, and **8**

	$\mathbf{8}[AsF_6]_2$	$\mathbf{8}SbF_6$	**8**
formula	$C_2As_2F_{12}N_4S_4$	$C_2F_6N_4S_4Sb$	$C_2N_4S_4$
a (Å)	12.7919(14)	6.523(2)	6.717(4)
b (Å)	9.5760(11)	7.780(2)	11.701(2)
c (Å)	18.532(2)	12.012(4)	8.269(3)
α (deg)	90	91.994(4)	90
β (deg)	104.034(2)	96.716(4)	106.69(3)
γ (deg)	90	109.177(4)	90
V (Å^3)	2202.3(4)	570.1(3)	622.6(4)
Z	6	2	4
space group	*Pn*	$P\bar{1}$	$P2_1/n$
cryst syst	monoclinic	triclinic	monoclinic
Color and habit	colorless, irregular	green, irregular	royal blue, needle
fw	586.14	444.05	208.29
T (K)	198	198	203
λ (Å)	0.71073	0.71073	0.71073
ρ_{calcd} (Mg/m^3)	2.652	2.587	2.222
μ (mm^{-1})	5.255	3.213	14.3
reflns collected	10 543	2740	2052
independent reflns	5315	1820	1822
R1, wR2	0.0334, 0.0823	0.0716, 0.1982	0.0526, 0.183
largest diff. peak, hole (e·Å^{-3})	1.246, −0.526	4.112, −1.558	0.73, −0.60

tion) with almost identical axis lengths and unit-cell volumes [622.6(4) and 612.8(2) Å^3, respectively] but with some minor variations in intermolecular contacts (explained below). When projected onto the *bc* plane, the crystal packing of $[\mathbf{8}]_2$ can be described as a herringbone-like motif of dimers with the molecules very closely packed with respect to each other (Figure 2A). Intermolecular lateral S···S and S···N contacts range from ca. 3.2 to 4.3 Å, which are very similar to the analogous interactions observed in the structure of **10**.[14b] Dimers $[\mathbf{8}]_2$ form columns down the *a* axis, in which intermolecular contacts range from ca. 3.6 to 3.7 Å (Figure 2B). The slippage of adjacent dimers along the long axis of the molecule is about 3°. The intracolumn interactions are similar to those in the structure of **10**, but the observed analogous slippage angle between the units of $[\mathbf{10}]_2$ is greater, that is, 18°.[14b]

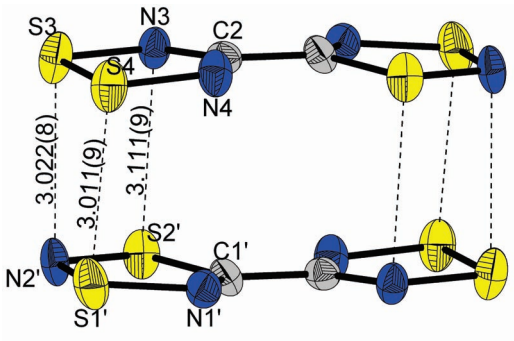

Figure 1. Representation of $[\mathbf{8}]_2$ with atom numbering as in the X-ray structure. Thermal ellipsoids are drawn at 50% probability.

The crystal structure of **8** coupled with the structural data for **10** may provide some important insights into the structure of the non-rearranged symmetric diradical **9**.[13] As noted

Table 5. Calculated Spin Densities, Hyperfine Coupling Constants[a] (MPW1PW91/gen) and NBO Charges [MPW1PW91/6-311+G(2df)] of **8**, $\mathbf{8}^{\bullet+}$, and $\mathbf{8}^{2+}$

	8				$\mathbf{8}^{\bullet+}$				$\mathbf{8}^{2+}$
	spin density	*a*, G (calcd)	*a*, G[b] (exp)	NBO charge	spin density	*a*, G (calcd)	*a*, G (exp)	NBO charge	NBO charge
C(1)	0.0272	0.46		0.0238	0.0137	1.62		0.0613	0.00806
N(1)	−0.0333	−0.48		−0.579	−0.0361	−0.54		−0.566	−0.541
S(1)	0.214	1.46		0.841	0.0272	0.47		1.18	1.28
N(2)	0.547	4.96	10.2	−0.896	0.0543	0.74	0.27[c]	−0.803	−0.754
S(2)	0.225	1.39		0.627	−0.00994	−0.73		0.938	1.01
C(2)	−0.141	−5.15		0.339	−0.105	−8.20		0.305	0.351
N(3)	0.298	2.44	4.7	−0.627	0.189	4.43	4.6	−0.586	−0.512
S(3)	0.292	1.97		0.468	0.274	4.70		0.581	0.864
S(4)	0.283	1.95		0.463	0.320	4.43		0.561	0.850
N(4)	0.288	2.20	4.7	−0.660	0.273	3.06	4.6	−0.673	−0.552

[a] Calculated for ^{13}C, ^{33}S, and ^{14}N isotopes. Gen is a basis set consisting of EPR-III for C and N atoms and TZVP for S atoms. Atom labeling scheme is given in Figure 1. [b] Coupling constants obtained directly from the spectra. [c] Obtained by simulation.

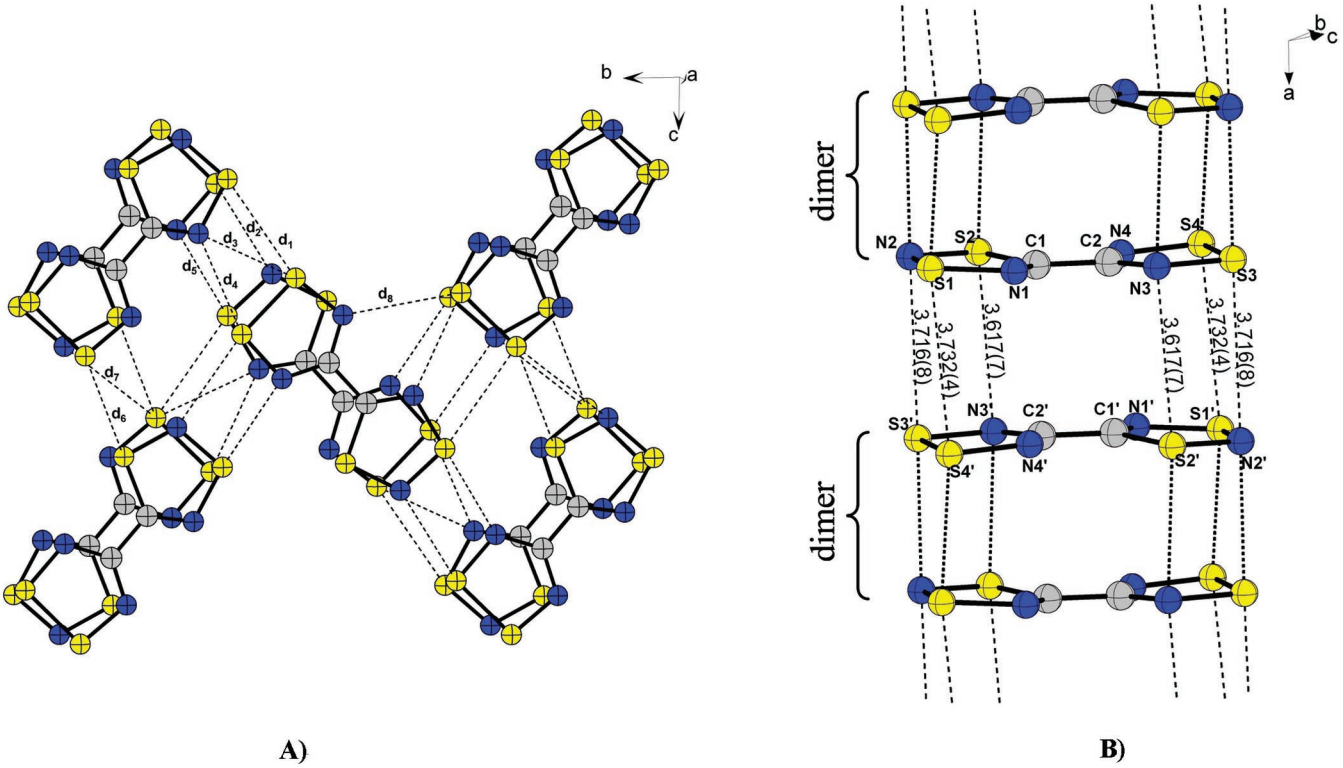

Figure 2. A) Unit cell of **8** projected down the *bc* plane. Lateral S···S and S···N contacts are illustrated as follows (Å): d1, 3.447(3); d2, 3.406(18); d3, 3.157(9); d4, 3.208(7); d5, 3.218(18); d6, 4.014(35); d7, 4.332(30); d8, 3.331(8). B) Illustration of the intrastack interactions between slipped dimers $[\mathbf{8}]_2$ along the *a* axis.

above, packing patterns of **8** and **10** are rather similar; that is, surprisingly, the replacement of the −CNSSN ring by the isomeric analog does not change the packing pattern of the diradicals. In light of newly available structural data, we can now suggest that **9** forms similar cofacial $\pi^*-\pi^*$ dimers, with the packing motif resembling those of **8** and **10**. We note that **9** is diamagnetic but undergoes a dramatic increase in paramagnetism upon grinding, interpreted as because of a second-order phase transition associated with the slippage of diradicals in the stacks.[13]

3.2.2. Crystal Structure of $8SbF_6$. The intramolecular bond distances and angles of $\mathbf{8}^{\bullet+}$ (Table 2) are similar to those in the corresponding rings in $[CNSNS]_2^{2+}$ [12b] and the −CNSSN• systems published in the literature.[1]

Radical cation $\mathbf{8}^{\bullet+}$ associates in the solid state, as was also observed for many other derivatives of the 1,2,3,5-dithiadiazolyls.[1] The centrosymmetric dimer of $\mathbf{8}^{\bullet+}$ is depicted in Figure 3. This trans cofacial mode of dimerization was previously observed for four derivatives of the RCNSSN• heterocycle.[28] Whereas in these neutral radicals it is the

(28) (a) Barclay, T. M.; Cordes, A. W.; George, N. A.; Haddon, R. C.; Itkis, M. E.; Oakley, R. T. *Chem. Commun.* **1999**, 2269. (b) Bricklebank, N.; Hargreaves, S.; Spey, S. E. *Polyhedron* **2000**, *19*, 1163. (c) Boeré, R. T.; Goh, L.-Y.; Ang, C. Y.; Kuan, S. L.; Lau, H. F.; Ng, V. W. L.; Roemmele, T. L.; Seagrave, S. D. *J. Organomet. Chem.* **2007**, *692*, 2697. (d) Hearns, N. G. R.; Hesp, K. D.; Jennings, M.; Korcok, J. L.; Preuss, K. E.; Smithson, C. S. *Polyhedron* **2007**, *26*, 2047.

(29) (a) Boeré, R. T.; Roemmele, T. L. *Coord. Chem. Rev.* **2000**, *210*, 369. (b) Boeré, R. T.; Moock, K. H. *J. Am. Chem. Soc.* **1995**, *117*, 4755.

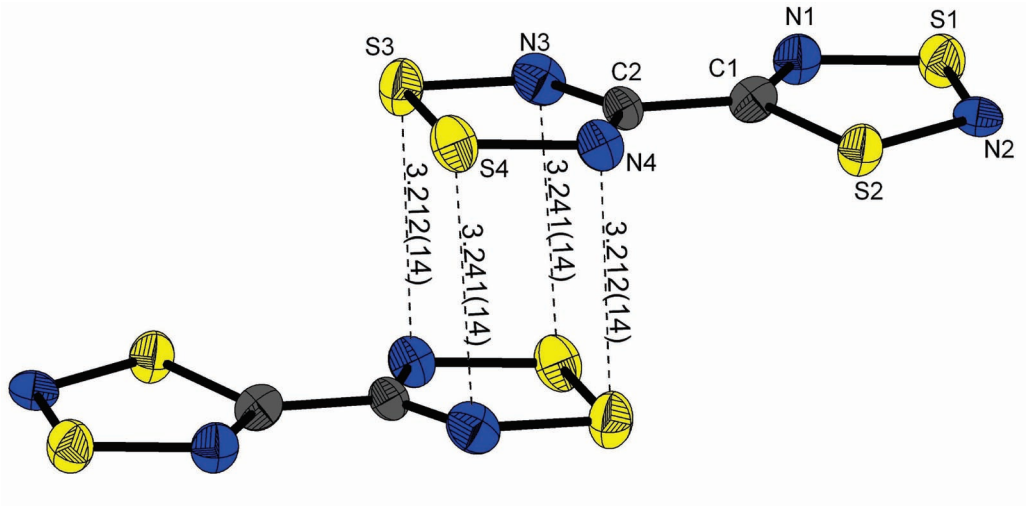

Figure 3. Depiction of centrosymmetric dimer $[\mathbf{8}^{\bullet+}]_2$. Thermal ellipsoids are drawn at 50% probability.

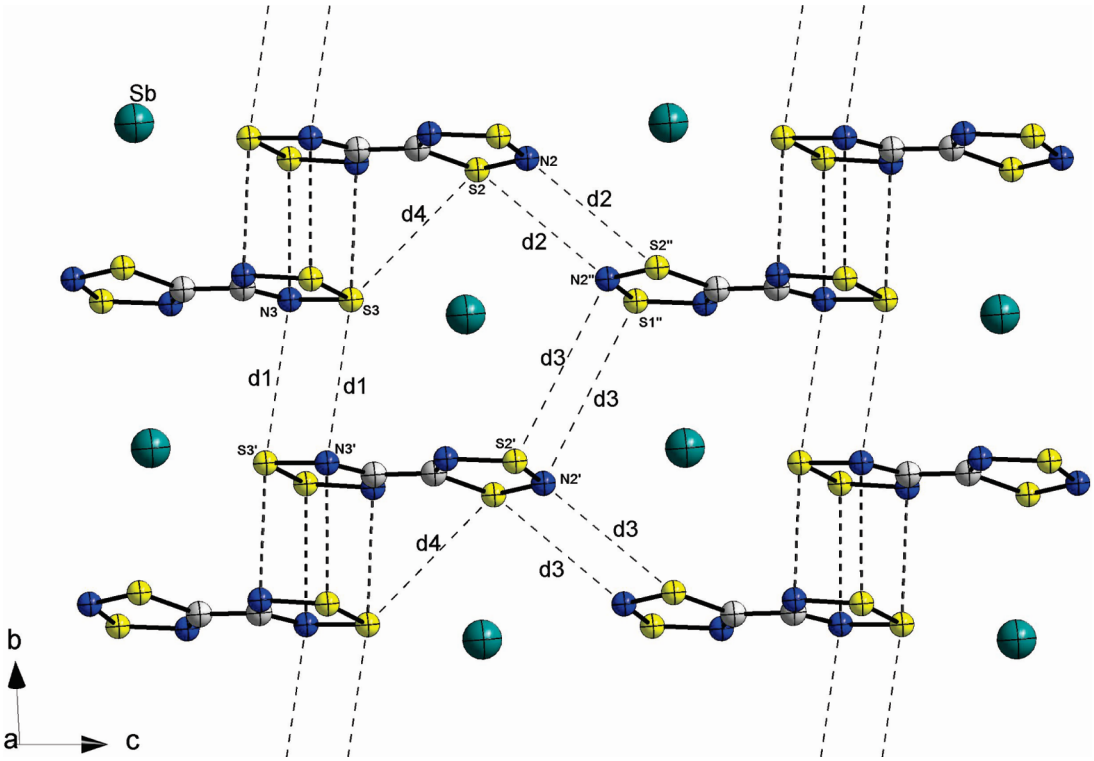

Figure 4. $a \times 2b \times 2c$ portion of the structure of $\mathbf{8}SbF_6$. Intermolecular distances are (Å): d1, 4.005(17); d2, 3.848(15); d3, 4.606(14); d4, 4.070(7). Anions are designated by an Sb atom for clarity.

substituent bulkiness that accounts for the observed dimeric conformations (bulky groups disfavor cofacial orientation), the trans cofacial mode of association in $[\mathbf{8}^{\bullet+}]_2$ appears to be a consequence of a coulombic repulsion between two positively charged $CNSNS^+$ rings. This is also demonstrated by the gas-phase calculations that show the conformation of $[\mathbf{8}^{\bullet+}]_2$, with the radical cations arranged in cis cofacial overlap, to be unstable with respect to two monomers (a more-detailed discussion is given in Section 3.7.2.).

The structure of $\mathbf{8}SbF_6$ contains SbF_6^- anions of distorted octahedral geometry (given in Figure S2A in the Supporting Information) and $\mathbf{8}^{\bullet+}$ cations arranged in an 8:8 coordination mode (Figure S3 in the Supporting Information). Six SbF_6^- anions reside closely in the region of the $-CNSNS^+$ moiety that carries most of the positive charge of the $\mathbf{8}^{\bullet+}$ molecule (Table 5).

Isolated dimers $[\mathbf{8}^{\bullet+}]_2$ are linked with other neighboring radical pairs via S···N contacts d1 (Figure 4) to produce chains along the *b* direction. In turn, these chains are interconnected with each other by means of electrostatic d2 and d3 interactions, forming layers of dimers in the *bc* plane. The SbF_6^- anions tend to situate in close proximity to the

(30) (a) MacLean, G. K.; Passmore, J.; Rao, M. N. S.; Schriver, M. J.; White, P. S.; Bethell, D.; Pilkington, R. S.; Sutcliffe, L. H. *J. Chem. Soc., Dalton Trans.* **1985**, 1405. (b) Banister, A. J.; Lavender, I.; Rawson, J. M.; Whitehead, R. J. *J. Chem. Soc., Dalton Trans.* **1992**, 1449.

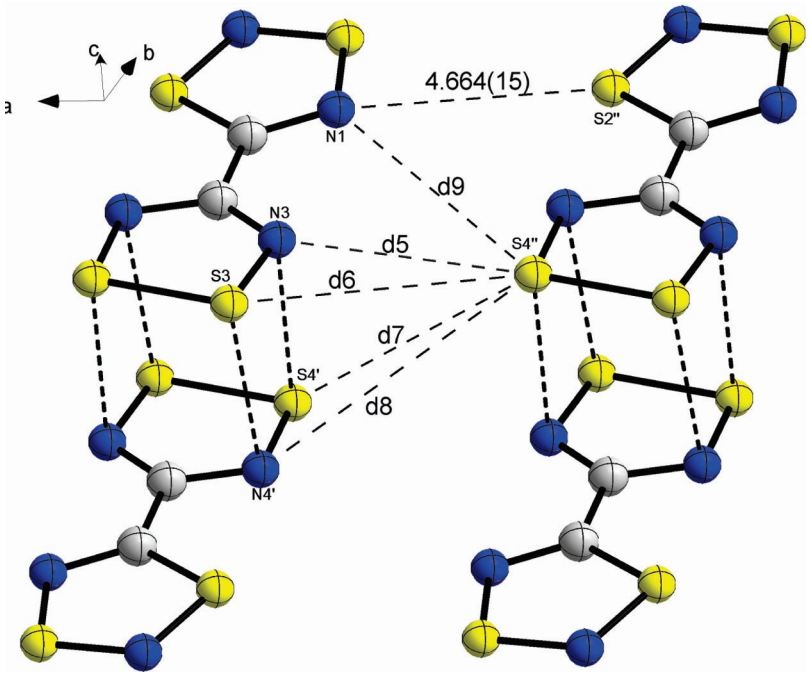

Figure 5. Diagram illustrating heterocyclic linkages between the layers of dimers $[\mathbf{8}^{\bullet+}]_2$. Intermolecular distances are (Å): d5, 3.857(14); d6, 4.899(8); d7, 4.091(9); d8, 4.800(18); d9, 3.819(14).

−CNSNS$^+$ molecular halves (visually appearing as tails of the radical cationic pairs) because of the larger positive charge carried by the tails (∑[NBO charges] = +0.81, Table 5). Figure 5 illustrates two $[\mathbf{8}^{\bullet+}]_2$ dimers that belong to two adjacent layers translated down the *a* axis. In this case, the favorable electrostatic S···N contacts cause a slippage of the layers with respect to each other, and the observed linkages (d5−d9) are long. These can be regarded as secondary directional forces.

Neutral RCNSSN• radicals typically exhibit a rich network of close intermolecular S···S and S···N interactions ranging from 3.0 to 3.6 Å.[1] However, the situation in **8**SbF_6 is somewhat special, taking into consideration the presence of anions in the lattice, which are absent in the neutral derivatives of 1,2,3,5-dithiadiazolyls. Substantially longer interdimeric heterocyclic contacts observed in the structure of **8**SbF_6 are therefore attributed to the dilution effect caused by diamagnetic SbF_6^- anions and electrostatic repulsions between the positively charged cations. The corresponding interradical S···N interactions in the neutral radicals are replaced by some favorable S···F contacts, the majority of which occurs in the spatial region of the −CNSNS$^+$ rings.

It is somewhat surprising to find that the intradimeric S••••N interactions between the two 1,2,3,5-dithiadiazolyl rings in $[\mathbf{8}^{\bullet+}]_2$ (∼3.2 Å) are almost identical to those found for the two neutral derivatives of the RCNSSN• heterocycle,[28a,b] exhibiting trans cofacial arrangement, despite the ionic nature of the structure of **8**SbF_6. This observation demonstrates the remarkable rigidity of the −$[CNSSN]_2$ dimeric unit in the structure of **8**SbF_6, even in the presence of the ionic crystal field.

The other known radical cations incorporating the −CNSSN• radical moiety are shown in Chart 3. In these

Chart 3

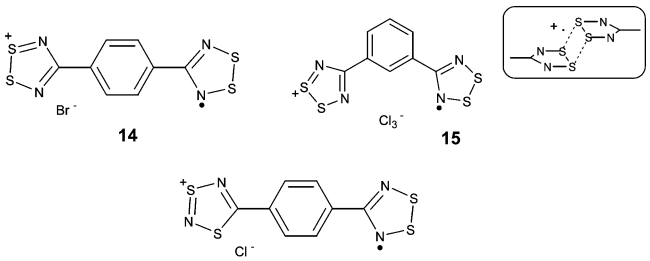

structures, the more-pronounced cation−anion interactions are expected to exist, given a relatively small size of the counter anions Br^-, Cl_3^-, and Cl^- as compared to that of the weakly coordinating SbF_6^- anion. *p*-Phenylene-substituted derivative **14** contains ribbonlike arrays of radical cations with no close cofacial interactions between the radical rings.[8a] This leads to paramagnetic behavior in the high-temperature regime. On the other hand, **15** contains an interesting structural unit that was designated as $[RCNSSN]_2^{\bullet+}$.[8b] The compound showed weakly paramagnetic behavior with an estimated exchange interaction of −465 cm^{-1} between the radical centers. Another radical cation incorporating the 1,2,3,5-dithiadiazolyl radical moiety, **16**,[8c] was not structurally characterized but showed a room temperature magnetic moment corresponding to about one unpaired spin per molecule, similar to that of **14**.

3.2.3. Crystal Structure of 8$[AsF_6]_2$. Figure 6 shows an essentially planar molecule of dication $\mathbf{8}^{2+}$ with mean internal structural parameters collected in Table 2 (the distorted AsF_6^- anion is depicted in Figure S2B in the Supporting Information). Bond distances and angles of $\mathbf{8}^{2+}$ are not different from those of $[CNSNS]_2^{2+}$ [12b] and other 1,2,3,5-dithiadiazolylium salts.[1a] The observed coordination numbers about each

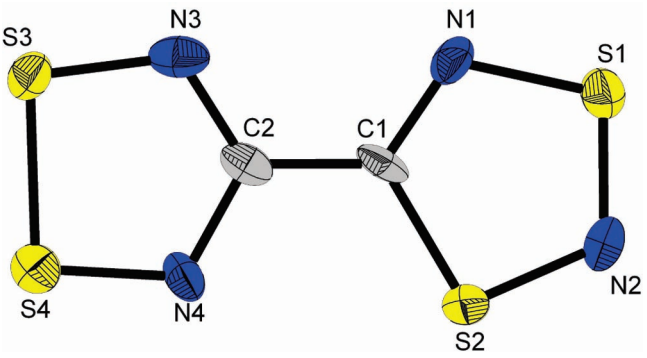

Figure 6. Depiction of 8^{2+}. Thermal ellipsoids are drawn at 50% probability.

dication and anion are 12 and 6, respectively (Figure S4 in the Supporting Information).

An interesting feature of the dication packing pattern is that along the *c* axis, chains are formed in which every third member is flipped in such a manner that the two isomeric moieties become adjacent to one another. The electrostatic S···N interactions within these chains are illustrated in Figure 7b.

3.3. Cyclic Voltammetry of $8[AsF_6]_2$, $8SbF_6$, and $9[SbF_6]_2$. The cyclic voltammograms of $\mathbf{8}^{\bullet+}$ and $\mathbf{9}^{2+}$ in a MeCN solution are depicted in Figure 8. Neutral **9** precipitated at room temperature, and slight warming produced the CV in Figure 8. Both compounds exhibit two reversible one-electron reductions [$\mathbf{8}^{2+}$, $E_{1/2}(+2/+1) = 1.033$ V; $E_{1/2}(+1/0) = 0.467$ V; $T = 298$ K; $\mathbf{9}^{2+}$, $E_{1/2}(+2/+1) = 0.786$ V; $E_{1/2}(+1/0) = 0.514$ V; T = 317 K; Table 4]. This is in contrast to $\mathbf{10}^{2+}$, where a single two-electron reduction wave was observed at +0.68 V.[14b] The redox processes of interest occurring in the systems are summarized in Schemes 3 and 4. In this reaction sequence, the presence of two distinct reversible CV waves is expected because of the sequential reduction of the $CNSSN^+$ [$E_{1/2}(+2/+1)$] and $CNSNS^+$ [$E_{1/2}(+1/0)$] rings. The larger separation between the potentials $E_{1/2}$ (+2/+1) and $E_{1/2}$ (+1/0) in $\mathbf{8}^{2+}$ (566mV) as compared to that of $\mathbf{9}^{2+}$ (272mV) is mirrored by our computational analysis of the frontier orbital energies of **8** (Figure 16, Section 3.7.1.) and **9**[13], and, in part, this enables the isolation of $\mathbf{8}^{\bullet+}$. Examination of the potentials listed in Table 4 suggests that $\mathbf{9}^{\bullet+}$ may also be isolable.

3.4. Vibrational Spectra of 8^{2+}, $8^{\bullet+}$, and 8. The relative simplicity of $\mathbf{8}^{2+}$, $\mathbf{8}^{\bullet+}$, and **8** makes it convenient to trace structural changes by vibrational spectroscopy. The low C_s symmetry of perfectly planar $\mathbf{8}^{2+}$, $\mathbf{8}^{\bullet+}$, and **8** leads to all of the 24 vibrational modes being both IR and Raman active. The DFT calculated and observed vibrational frequencies of the series are in excellent agreement and are compiled in Table 1.

The calculated C−C stretching modes of $\mathbf{8}-\mathbf{8}^{2+}$ (Table 1) vary slightly in magnitude; however, their correlation with the C−C bond distances is ambiguous, owing to the heavily mixed character of the C−C stretch with the C−N vibrational modes.

Almost no change in the C_2-N_3 and C_2-N_4 frequencies is observed, in agreement with the little structural changes in the series $\mathbf{8}-\mathbf{8}^{2+}$. There is a slight decrease in the C_1-N_1 bond distance upon the reduction of $\mathbf{8}^{\bullet+}$ into **8** (calcd values are 1.297 and 1.278 Å, respectively), which is manifested in a small change in the corresponding stretching frequency (calcd ca. 60 cm^{-1}).

On the other hand, because most of the frontier orbital electron density resides on the S_2N_2 moieties, we can expect stretching frequencies associated with these structural fragments to undergo significant shifting. Upon reduction of $\mathbf{8}^{2+}$, the unpaired electron transfers to the −CNSSN ring. In the resultant radical cation $\mathbf{8}^{\bullet+}$, the bond distances of the CNSSN moiety [S_3-N_3, S_4-N_4, S_3-S_4] elongate (Table 2), shifting the corresponding stretching frequencies to lower values [$\delta_s(N_3S_3S_4N_4)$ ip, $\delta_{as}(N_3S_3S_4N_4)$ ip, and $\nu(S_3-S_4)$ modes in Table 1]. From the first reduction step, there is little change in the vibrational modes of the chemically intact $CNSNS^+$ cationic ring. As expected, the stretching frequencies of this ring decrease in magnitude when $\mathbf{8}^{\bullet+}$ is further reduced to the neutral diradical **8** [$\nu(S_2-N_2)$, $\nu(S_1-N_1)$, $\delta_{as}(S_2N_2S_1)$ ip, and $\delta(S_2N_2S_1)$ oop stretching modes in Table 1], correlating with lengthening of the corresponding bond distances.

Whereas we did not observe any peaks belonging to **10** in the IR spectrum of **8**, there were unassigned bands in the vibrational spectra of $\mathbf{8}^{2+}$, $\mathbf{8}^{\bullet+}$, and **8** (1120 (ms), 977 (vw) and 1092 (ms), and 1047 (w) cm^{-1}, respectively). The origin of these bands is not clear. All of the other modes were assigned to $\mathbf{8}[AsF_6]_2$, $\mathbf{8}[AsF_6]$, and **8**.

3.5. EPR Studies. 3.5.1. EPR Spectrum of $8SbF_6$ in SO_2 Solution. $\mathbf{8}SbF_6$ redissolved in SO_2 gave an EPR spectrum consisting of five lines with $a = 4.6$ G (Figure 9) as a consequence of hyperfine interaction with two equivalent nitrogen nuclei ($I = 1$). A summary of experimental and calculated data is provided in Table 5. The *g* value of $\mathbf{8}^{\bullet+}$ is rather similar to those of other $RCNSSN^{\bullet}$ radicals.[1a,d] The a_N value of 4.6 G is somewhat close to those obtained for the $RCNSSN^{\bullet}$ with electronegative substituents (e.g., R = F_3C, F; $a_N = 5.1$ G[31a]). Hyperfine coupling with the ^{14}N atoms of the $-CNSNS^+$ ring is not directly observed; however, a small a_N of 0.27 G (an upper limit) is inferred by simulating the observed spectra (Table 5). Little delocalization of spin density away from the $-CNSSN^{\bullet}$ heterocyclic ring is also reflected in the analysis of the frontier molecular orbitals of $\mathbf{8}^{\bullet+}$ (Figure 16, Section 3.7.1.).

We note that the DFT-calculated hyperfine coupling constants of N3 and N4 are nonequivalent (ca. 1.4 G difference, Table 5), seemingly contradicting experimental EPR results that show a five-line pattern typical of the $RCNSSN^{\bullet}$ radical system[1a,d] with two equivalent nitrogen atoms. This suggests that the real nitrogen hyperfine coupling constants in solution are somewhat closer to one another than the calculated values, or, alternatively, there might be a rapid rotation around the C−C bond, which makes both nitrogen atoms (N3 and N4) equivalent. However, the latter hypothesis

(31) (a) Höfs, H. U.; Bats, J. W.; Gleiter, R.; Hartmann, G.; Mews, R.; Eckert-Maksic, M.; Oberhammer, H.; Sheldrick, G. M. *Chem. Ber.* **1985**, *118*, 3781. (b) Fairhurst, S. A.; Johnson, K. M.; Sutcliffe, L. H.; Preston, K. F.; Banister, A. J.; Hauptman, Z. V.; Passmore, J. *J. Chem. Soc., Dalton Trans.* **1986**, 1465.

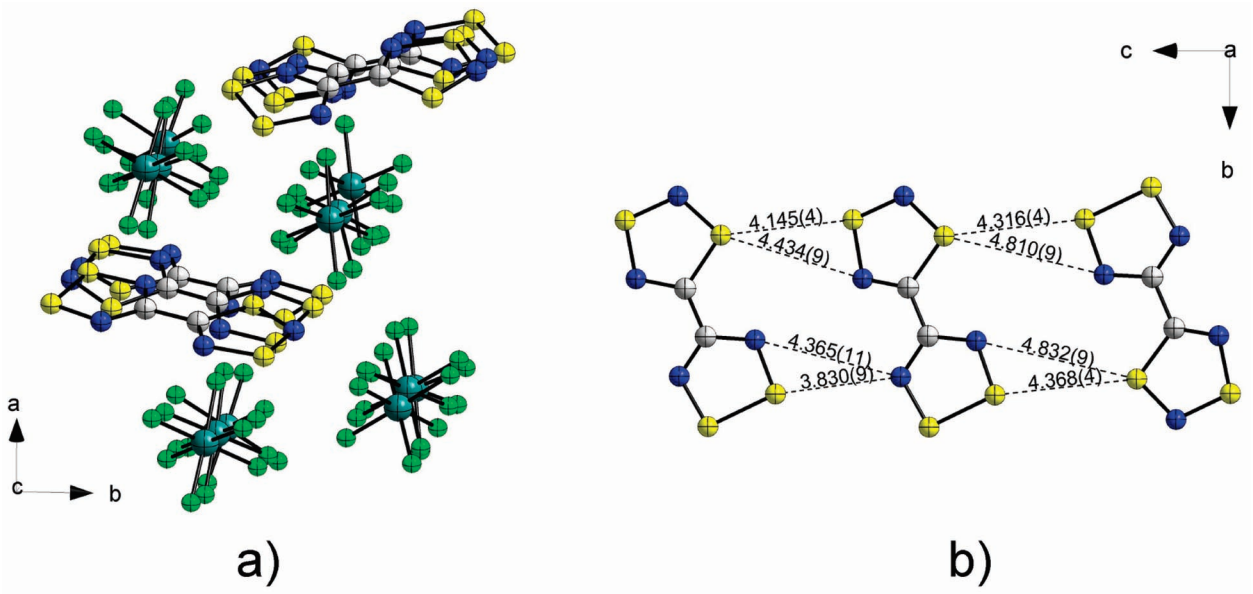

Figure 7. a) Unit cell of **8**$[AsF_6]_2$. b) Representative chain of $\mathbf{8}^{2+}$ in the *bc* plane.

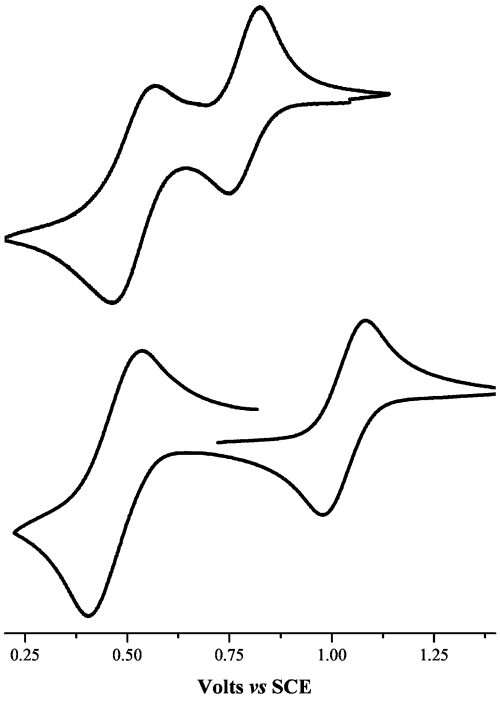

Figure 8. Cyclic voltammogram of $\mathbf{8}^{\bullet+}$ (bottom) and $\mathbf{9}^{2+}$ (top).

is not supported by our potential energy scan calculations of the intramolecular rotation about the C−C bond, which give a rotation barrier of ca. 30 kJ/mol (Figure 17) in the gas phase. However, it is possible that this barrier may be reduced upon solvation, where the rotamer could be stabilized by cation−anion contacts of a $\mathbf{8}^{\bullet+}\cdots SbF_6^-$ ion pair, and the ring wobbling around the C−C bond contributes to the averaging of the two coupling constants (equal to 2.7 G for the 90° rotamer, according to calculations).

The frozen-solution EPR spectrum of **8**SbF_6 in SO_2 (Figure 10) showed a typical anisotropic pattern of the RCNSSN• ring system.[1d] No splittings were observed at the *x* component, and the *y* component showed features reminiscent of those seen in the frozen-solution EPR spectrum of PhCNSSN•.[31b] The major anisotropic hyperfine coupling along the *z* axis (normal to the plane of the radical ring) is split into five lines, reflecting the p_z nature of the two N atoms carrying most of the spin density. This also indicates that in the absence of rotation or molecular tumbling the two N3 and N4 atoms are still equivalent in the frozen solution on the time scale of EPR measurements. Alternatively, this EPR spectrum could arise from the rotamer, in which the two rings are rotated 90° with respect to one another and stabilized by the ionic $S^{\delta+}\cdots F^{\delta-}$ interaction from SbF_6^- anions in a $\mathbf{8}^{\bullet+}\cdots SbF_6^-$ ion pair that replace the favorable $S^{\delta+}\cdots N^{\delta-}$ contacts in the planar conformation.

We note that the frozen-solution spectrum of **8**SbF_6 is almost identical to that observed for the PhCNSSN• radical, in which there seems to be little spin-density delocalization onto the substituent group.[31b]

3.5.2. In Situ EPR Studies of the Rearrangement of 8 into 10 in an SO_2 Solution. A series of EPR spectra (Figure 11) were obtained in situ upon the reduction of **8**SbF_6 with a mixture of $SbPh_3$ and NBu_4Cl (used instead of $FeCp_2$, that is itself oxidized into the EPR active ferrocenium cation). Similar EPR spectra were recorded after redissolution of a sublimed sample of **8** in SO_2.

The complex appearance of the spectra suggests the presence of more than one radical species. Careful analysis of the spectra coupled with simulation data gives a representation of the mixture as a combination of pentet and triplet lines. The intensity of the pentet lines is considerably greater than that of the triplet. We propose that the former is actually a superposition of the integral areas from the *three* −CNSSN• radical rings belonging to diradicals **8** and **10**. Their *g* factors are expected to be almost identical [measured as 2.009(1)]; hence, yielding only a *single* pentet. On the other hand, the intensity of the triplet lines [$g = 2.004(1)$] was somewhat weaker, and it continuously decreased over time, indicating the rather fast rearrangement of **8** into **10** (Figure 11). By simulating each EPR spectrum of the mixture, it was possible

Table 4. Selected Electrochemical Data of Difunctional RCNSSN and RCNSSN Ring Systems[a]

compound	process	potential, V versus SCE	$E_{1/2}(+2/+1)$- $E_{1/2}(+1/0)$, V	ref
$\mathbf{8}^{\cdot+}$	+1/0	+0.465	0.560	this work
	+2/+1	+1.025		
$\mathbf{8}^{2+}$	+1/0	+0.467	0.566	this work
	+2/+1	+1.033		
$\mathbf{9}^{2+}$	+1/0	+0.514	0.272	this work
	+2/+1	+0.786		
$\mathbf{10}^{2+}$	+2/0	+0.68	N/A	14b
[*p*-NSSNC−C_6H_4-CNSSN]$^{2+}$	+2/0	+0.61	N/A	29a
[*m*-SNSNC−C_6H_4-CNSSN]$^{2+}$	+1/0	+0.387	0.260	8c
	+2/+1	+0.647		
[*p*-SNSNC−C_6H_4-CNSSN]$^{2+}$	+1/0	+0.303	0.292	30b
	+2/+1	+0.595		
p-C_6H_4[CNSNS]$_2^{2+}$	+2/0	+0.224	N/A	24

[a] Comprehensive compilation is provided in Tables 7 and 8 of ref 29a. Acetonitrile solutions. Reversible processes.

Scheme 3

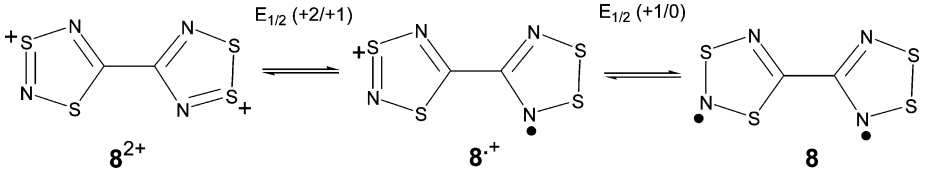

Scheme 4

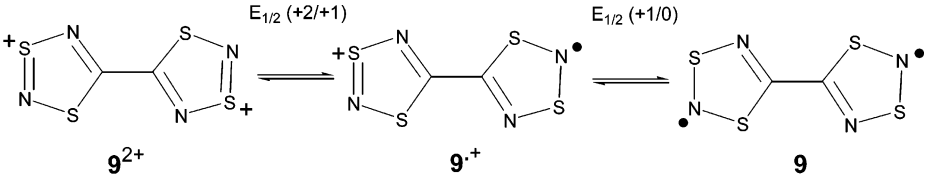

to determine and compare relative ratios of integral areas of pentet and triplet species, from which relative concentrations of **8** and **10** were calculated (Table S5 in the Supporting Information). The obtained data plotted as (% of **8**) versus time (Figure S5 in the Supporting Information) indicate that after about 1.5 h the transformation of **8** into **10** is almost complete, and the triplet lines are barely distinguishable in the spectrum.

The hyperfine coupling constant of the −CNSNS• radical rings (10.2 G) determined experimentally from the $t = 8$ min EPR spectrum is similar to those found for the other RCNSNS• radicals.[12a,13,32] This coupling has previously been assigned to the terminal N atom, and therefore we assign it to N2 of diradical **8**. The observed hyperfine coupling constant of the pentet line was 4.7 G, somewhat smaller than the value of 5 G reported for **10** in $CHCl_3$.[14b]

In an EPR spectrum of **8** (Figure 11), the areas of the pentet and triplet lines are simply additive contributions of two monoradical rings, implying no exchange coupling between the radical centers. This is evidenced by the absence of any features in the EPR spectrum of **8** assignable to the

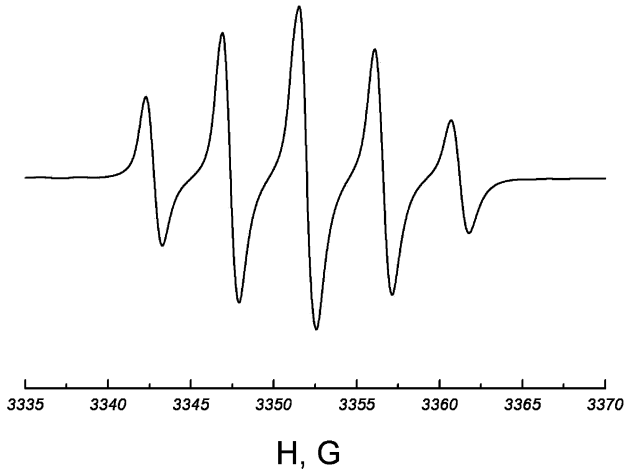

Figure 9. Experimental spectrum of **8**SbF_6 at 213 K in SO_2 [$g = 2.011$ (1), $a_N = 4.6$ G]. The simulated spectrum is included in the Supporting Information.

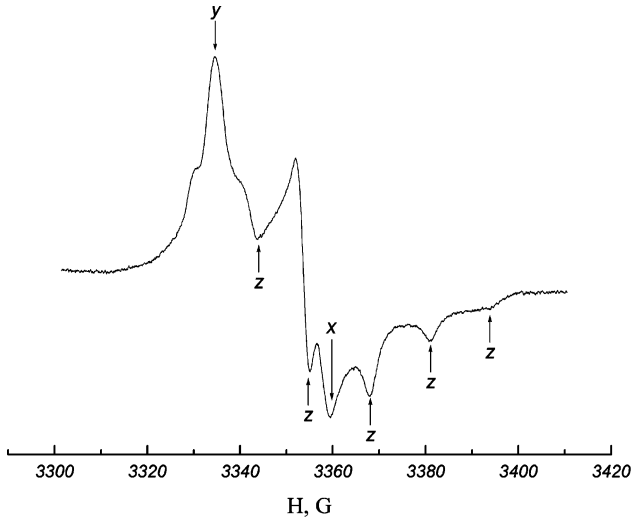

Figure 10. X-band EPR frozen-SO_2-solution spectrum of **8**SbF_6 at 108 K.

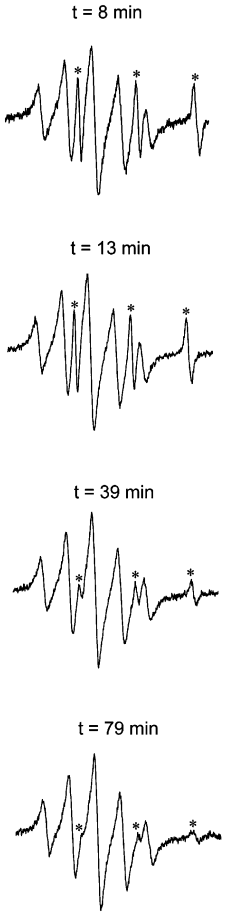

Figure 11. EPR spectra of a SO_2 solution of **8** as a function of time, showing the rearrangement into **10**. Lines originating from the −CNSNS• ring are marked with an asterisk. *g* factor (pentet) = 2.009(1); *g* factor (triplet) = 2.004(1). Experimental and calculated hyperfine coupling constants are given in Table 5. Simulated spectra are included in the Supporting Information.

$S = 1$ state, that is, zero-field splitting components and the half-field transition. Consistent with the very small communication between unpaired electrons, the experimental ^{14}N hyperfine coupling constants (Table 5) and *g* factors of **8** are very similar to those of the corresponding isolated RCNSSN• and RCNSNS• radicals previously published in the literature.[1a,d]

We note that the EPR spectrum of related diradical **9**[13] was also consistent with two noninteracting unpaired spins. However, rearranged analog **10**[14b] showed the onset of a small exchange interaction at elevated temperatures (303 K). Distinct zero-field splitting components were resolved for $\mathbf{11}^{2+}$,[33] which is isolobal to **8**−**10**. Interestingly, evidence for intramolecular coupling in 1,3- and 1,4-phenylene-bridged bis(1,2,3,5-dithiadiazolyl) diradicals[34,35] has been reported, despite the longer distance between the radicals centers. It could be that the lack of $S = 1$ components in the EPR spectra of **8** and **9** is due to intrinsic spectroscopic features pertaining to the dipolar exchange interaction, for example molecular tumbling in solution or intramolecular spin relaxation effects. To prove this hypothesis, more-sophisticated and detailed EPR studies are necessary.

3.5.3. Solid-state EPR of $8SbF_6$ and 8. Recently, we reported that the sulfur−nitrogen radical dimers $[ClCNSSS]_2^{2+}$ [11a] and $C_4F_8[CNSSS]_2^{2+}$ [11b] showed thermally excited triplet states $S = 1$ at room temperature and 280 K, respectively. These phenomena, while described for a few other organic−radical pairs,[43c,44a,45,47] were not previously observed for any of the thiazyl radical family, partly because of their known tendency to strongly associate in the solid state, especially for the RCNSSN• ring system. We previously proposed[11a]

(32) (a) Burford, N.; Passmore, J.; Schriver, M. J. *J. Chem. Soc., Chem. Commun.* **1986**, 140. (b) Aherne, C.; Banister, A. J.; Luke, A. W.; Rawson, J. M.; Whitehead, R. J. *J. Chem. Soc., Dalton Trans.* **1992**, 1277.

(33) (a) Berces, A.; Enright, G. D.; Mclaurin, G. E.; Morton, J. R.; Preston, K. F.; Passmore, J.; Wood, D. J. *Magn. Reson. Chem.* **1999**, *37*, 353. (b) Boyle, P. D.; Cameron, T. S.; Decken, A.; Grein, F.; Knapp, C.; Mawhinney, R. C.; Palacio, F.; Passmore, J.; Rautiainen, J. M.; Shuvaev, K. V.; Thompson, R. C.; Wood, D. J. *Inorg. Chem.* **2007**, manuscript in preparation.

(34) Beekman, R. A.; Boeré, R. T.; Moock, K. H.; Parvez, M. *Can. J. Chem.* **1998**, *76*, 85.

(35) (a) Andrews, M. P.; Cordes, A. W.; Douglass, D. C.; Fleming, R. M.; Glarum, S. H.; Haddon, R. C.; Marsh, P.; Oakley, R. T.; Palstra, T. T. M.; Schneemeyer, L. F.; Trucks, G. W.; Tycko, R. R.; Waszczak, J. V.; Warren, W. W.; Young, K. M.; Zimmerman, N. M. *J. Am. Chem. Soc.* **1991**, *113*, 3559. (b) Cordes, A. W.; Haddon, R. C.; Oakley, R. T.; Schneemeyer, L. F.; Waszczak, J. V.; Young, K. M.; Zimmerman, N. M. *J. Am. Chem. Soc.* **1991**, *113*, 582.

(36) Bleaney, B.; Bowers, K. D. *Proc. R. Soc. London* **1952**, *A214*, 451.

(37) The values of parameters for **8** given herein are slightly different from those given in ref 15 due to use of different software (program *MAGNET* custom-made by J. M. Rawson and *SigmaPlot 8.0* used in the present article). The magnitude of both sets of parameters is the same, to the first order of approximation.

(38) (a) Cordes, A. W.; Haddon, R. C.; Hicks, R. G.; Kennepohl, D. K.; Oakley, R. T.; Schneemeyer, L. F.; Waszczak, J. V. *Inorg. Chem.* **1993**, *32*, 1554. (b) Bryan, C. D.; Cordes, A. W.; Haddon, R. C.; Hicks, R. G.; Kennepohl, D. K.; MacKinnon, C. D.; Oakley, R. T.; Palstra, T. T. M.; Perel, A. S.; Scott, S. R.; Schneemeyer, L. F.; Waszczak, J. V. *J. Am. Chem. Soc.* **1994**, *116*, 1205. (c) Bryan, C. D.; Cordes, A. W.; Fleming, R. M.; George, N. A.; Glarum, S. H.; Haddon, R. C.; MacKinnon, C. D.; Oakley, R. T.; Palstra, T. T. M.; Perel, A. S.; Schneemeyer, L. F.; Waszczak, J. V. *J. Am. Chem. Soc.* **1995**, *117*, 6880. (d) Barclay, T. M.; Cordes, A. W.; de Laat, R. H.; Goddard, J. D.; Haddon, R. C.; Jeter, D. Y.; Mawhinney, R. C.; Oakley, R. T.; Palstra, T. T. M.; Patenaude, G. W.; Reed, R. W.; Westwood, N. P. C. *J. Am. Chem. Soc.* **1997**, *119*, 2633. (e) Barclay, T. M.; Cordes, A. W.; George, N. A.; Haddon, R. C.; Oakley, R. T.; Patenaude, G. W.; Reed, R. W.; Zhang, H. *Chem. Commun.* **1997**, 873. (f) Barclay, T. M.; Cordes, A. W.; Haddon, R. C.; Itkis, M. E.; Oakley, R. T.; Reed, R. W.; Zhang, H. *J. Am. Chem. Soc.* **1999**, *121*, 969.

(39) Diradical character is not an absolute measure but rather a relative one that can be used to compare the diradical species with one another. The diradical character calculated from the orbital occupancies gives an upper limit for the diradical character since the frontier orbital occupancies include small contributions due to excitations from lower orbitals.

(40) (a) Döhnert, D.; Koutecky, J. *J. Am. Chem. Soc.* **1980**, *102*, 1789. (b) Jung, Y.; Head-Gordon, M. *J. Phys. Chem. A.* **2003**, *107*, 7475. (c) Jung, Y.; Head-Gordon, M. *ChemPhysChem.* **2003**, *4*, 522. (d) Aikens, C.; Gordon, M. S. *J. Phys. Chem. A* **2003**, *107*, 104. (e) Bendikov, M.; Duong, H. M.; Starkey, K.; Houk, K. N.; Carter, E. A.; Wudl, F. *J. Am. Chem. Soc.* **2004**, *126*, 7416.

(41) All of the calculations were single point. In $[\mathbf{8}]_2$, half of the dimer was manually removed, and the broken C−C bonds were replaced by the C−Cl bonds. Therefore, the quoted number of diradical character of $[\mathbf{8}]_2$ refers to these [ClCNSSN···NSNSCCl] dimeric units.

(42) (a) Niecke, E.; Fuchs, A.; Baumeister, F.; Nieger, M.; Schoeller, W. W. *Angew. Chem., Int. Ed. Engl.* **1995**, *34*, 555. (b) Scheschkewitz, D.; Amii, H.; Gornitzka, H.; Schoeller, W. W.; Bourissou, D.; Bertrand, G. *Science* **2002**, *295*, 1880. (c) Cui, C.; Brynda, M.; Olmstead, M. M.; Power, P. P. *J. Am. Chem. Soc.* **2004**, *126*, 6510. (d) Cox, H.; Hitchcock, P. B.; Lappert, M. F.; Pierssens, L. J.-M. *Angew. Chem. Int. Ed.* **2004**, *43*, 4500. (e) Tuononen, H. M.; Suontamo, R.; Valkonen, J.; Laitinen, R. S. *J. Phys. Chem. A* **2004**, *108*, 5670.

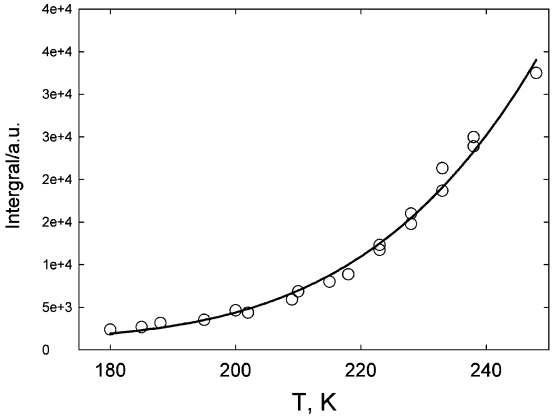

Figure 12. Temperature dependence of the double-integral EPR intensity of **8**SbF_6 in the solid state (○) and its fit to the Bleaney−Bowers model[36] (—). The double-integrated line of the spectrum used in the fitting is marked with an asterisk in Figure 13. The actual numerical data are given in Table S1 in the Supporting Information.

that thermally exited triplet states could potentially be detected in many other thiazyl radical dimers by variable-temperature EPR studies of the solids. Herein, we provide further evidence of the generality of such phenomena, by characterizing the $S = 1$ state in dimer $[\mathbf{8}^{\bullet+}]_2$. As was the case for $C_4F_8[CNSSS]_2[AsF_6]_2$ solid,[11b] **8**SbF_6 showed only one broad line at room temperature. However, upon cooling the sample to ca. 200 K, a well-resolved EPR spectrum was observed, with the characteristic dipolar splitting components of the $S = 1$ state (Figure 13), which were unobservable at room temperature as a result of line-broadening effects. The zero-field splitting parameters [$|D| = 0.0267(6)$ cm^{-1}, $|E| = 0.0012(1)$ cm^{-1}] were directly extracted from the spectra and appeared to be similar to those recorded for $[ClCNSSS]_2^{2+}$ [11a] and the radical pairs found in the solid $C_4F_8[CNSSS]_2$-$[AsF_6]_2$.[11b] The half-field transition $\Delta M_s = \pm 2$ was also detected. Upon further cooling, the intensity of the triplet lines decreased and eventually disappeared below 123 K, leaving only the $S = {}^1/_2$ signal (Figure 13). This behavior is essentially the same as that previously observed for analogous systems[11] and is typical of the thermally occupied triplet state in a dimer of two antiferromagnetically coupled spins. The temperature dependence of the double-integral intensity of the triplet components fitted to the Bleaney−Bowers model[36] (Figure 12) gave a singlet−triplet gap of $[\mathbf{8}^{\bullet+}]_2$ as -1800 ± 100 cm^{-1} (-22 ± 1 kJ/mol). This value is close to -1900 ± 100 cm^{-1} (-23 ± 1 kJ/mol) found for $[ClCNSSS]_2^{2+}$.[11a] If it can be assumed that the in situ dimerization energy of the monomer is ca. half of the singlet−triplet gap in the dimer, then the dimerization energy of $[\mathbf{8}^{\bullet+}]_2$ is ca. -11 kJ/mol. The magnitude of the singlet−triplet splitting is dependent on the various factors including the extent of mixing between two overlapping SOMOs, which can be qualitatively traced by quantum-chemical calculations (Section 3.7.1.).

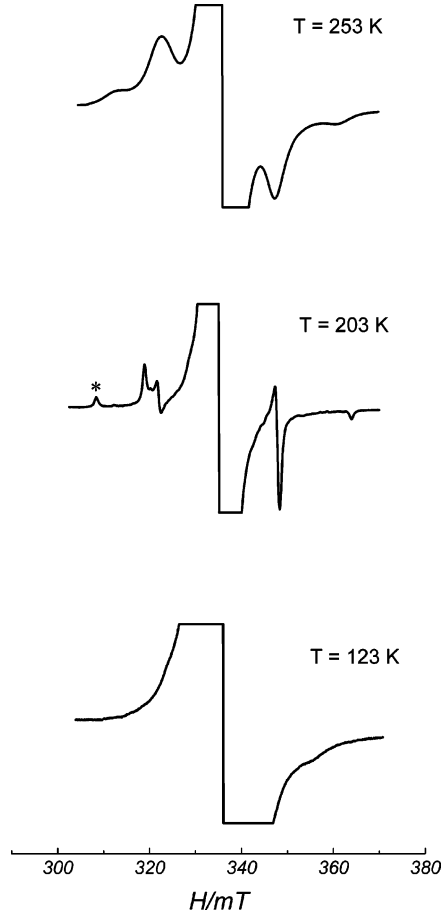

Figure 13. Temperature-dependent transformation of the solid-state X-band EPR spectra of **8**SbF_6. $S = 1$, $g_{xx} = 2.008(1)$, $g_{yy} = 2.019(1)$, $g_{zz} = 2.004(1)$; $S = {}^1/_2$, $g_{(iso)} = 2.011(1)$.

Similar to the previously studied AsF_6^- salts of $[ClCNSSS]_2^{2+}$ and $C_4F_8[CNSSS]_2^{2+}$, **8**SbF_6 exhibited a strong signal in the middle of the EPR spectrum that was assigned to the $S = {}^1/_2$ lattice-defect sites, arising from the occasional absence of the radical half of the dimeric pairs. Notably, the g factor of this signal was identical to that of $\mathbf{8}^{\bullet+}$ in solution (vide supra).

In contrast to **8**SbF_6, which exhibited very well-resolved ZFS components, only the $S = {}^1/_2$ signal was detected in the solid-state sample of **8** in the accessible temperature range of 103−473 K. No lines attributable to the $S = 1$ state (including the half-field transition) were observed. In $[\mathbf{8}]_2$, the singlet−triplet splitting ($2J$) should be substantially larger, because the intradimeric contacts in this dimer are ca. 3 Å, that is, about 0.2 Å shorter than those found in $[\mathbf{8}^{\bullet+}]_2$. Shortening of the S···S and S···N interactions should lead

(43) (a) Goto, K.; Kubo, T.; Yamamoto, K.; Nakasuji, K.; Sato, K.; Shiomi, D.; Takui, T.; Kubota, M.; Kobayashi, T.; Yakushi, K.; Ouyang, J. *J. Am. Chem. Soc.* **1999**, *121*, 1619. (b) Koutentis, P. A.; Chen, Y.; Cao, Y.; Best, T. P.; Itkis, M. E.; Beer, L.; Oakley, R. T.; Cordes, A. W.; Brock, C. P.; Haddon, R. C. *J. Am. Chem. Soc.* **2001**, *123*, 3864. (c) Morita, Y.; Aoki, T.; Fukui, K.; Nakazawa, S.; Tamaki, K.; Suzuki, S.; Fuyuhiro, A.; Yamamoto, K.; Sato, K.; Shiomi, D.; Naito, A.; Takui, T.; Nakasuji, K. *Angew. Chem., Int. Ed.* **2002**, *41*, 1793.
(44) (a) Guirauden, A.; Johannsen, I.; Batail, P.; Coulon, C. *Inorg. Chem.* **1993**, *32*, 2446 and references therein. (b) Yamazaki, D.; Nishinaga, T.; Tanino, N.; Komatsu, K. *J. Am. Chem. Soc.* **2006**, *128*, 14470. (c) Miller, L. L.; Mann, K. R. *Acc. Chem. Res.* **1996**, *29*, 417. (d) Nishinaga, T.; Komatsu, K. *Org. Biomol. Chem.* **2005**, *3*, 561.
(45) Hove, M. J.; Hoffman, B. M.; Ibers, J. A. *J. Chem. Phys.* **1972**, *56*, 3490.
(46) (a) Miller, J. S.; Novoa, J. J. *Acc. Chem. Res.* **2007**, *40*, 189. (b) Del, Sesto, E.; Miller, J. S.; Lafuente, P.; Novoa, J. J. *Chem.—Eur. J.* **2002**, *8*, 4894.
(47) Coulon, C.; Clerac, R. *Chem. Rev.* **2004**, *104*, 5655 and references therein.

Table 6. Compilation of Experimental Data on the Exchange Interactions in Thiazyl Radical Dimers[a]

thiazyl dimer	intradimeric distance at 200 K (Å)	ΔE_{ST} [EPR][b] (cm^{-1})	ΔE_{ST} [Mag] (cm^{-1})	$\|D\|/\|E\|$, cm^{-1}	ref
$[ClCNSSS]_2^{2+}$	3.167(2)	-1900 ± 100		0.0250(6)/ 0.0012(6)	11a
$[\text{-}C_4F_8\text{-}CNSSS]_2^{2+}$ [c]	3.306(2)	-900 ± 90	-910 ± 70	0.0254(8)/ 0.0013(8)	11b
$[\text{-}C_2F_4\text{-}CNSSS]_2^{2+}$ [c]	3.455(1)		-500 ± 30		11b
$[\mathbf{8}^{\bullet+}]_2$	ca. 3.2[d]	-1800 ± 100		0.0267(6)/ 0.0012(1)	this work

[a] The only other unambiguously characterized triplet state in the thiazyl radical chemistry was reported for diradical $\mathbf{11}^{2+}$ ($|D| = 0.01975(1)$ cm^{-1}, $|E| = 0.000683(1)$ cm^{-1} (ref 33). [b] Abbreviations ΔE_{ST} [EPR] and ΔE_{ST} [Mag] stand for singlet−triplet gaps extracted from variable-temperature solid-state EPR and magnetic susceptibility measurements, respectively. [c] These radical pairs were found in solids $C_4F_8[CNSSS]_2[AsF_6]_2$ and $C_2F_4[CNSSS]_2[AsF_6]_2$, respectively. [d] Note that types of SOMO−SOMO interactions in the top three compounds and $\mathbf{8}SbF_6$ are different, and therefore the intramolecular distances are not directly comparable.

to stronger bonding between the radical centers, thus increasing the singlet−triplet gap. This is supported by quantum-chemical calculations, which indicated the larger magnitude of the singlet−triplet gap for $[\mathbf{8}]_2$ compared to that of $[\mathbf{8}^{\bullet+}]_2$ (Section 3.7.3). A priori elevated temperature conditions increase the occupation of the triplet state, according to the Boltzmann distribution relation. However, heating to 473 K did not afford any signals attributable to the $S = 1$ states. We propose that the absence of triplet features in **8** is most likely caused by line-broadening effects arising from the thermally induced lattice vibrations. Alternatively, the ZFS components are likely to merge with the area of the intense doublet signal that has a considerably larger line width at higher temperatures. This line broadening can be a consequence of increased exchange interactions between the lattice-defect $S = {}^1/_2$ sites, as a result of the breakage of dimeric units. Therefore, it appears that the triplet states in the dimers with large singlet−triplet gaps ($|2J| > 2000$ cm^{-1}) may not be observable at higher temperatures. From the previously known results and our newly obtained data on $[\mathbf{8}^{\bullet+}]_2$ (compiled in Table 6), we can tentatively establish the lowest and the highest benchmarks, within the limit of which it is feasible to resolve ZFS components. Our proposed range constitutes 900 $cm^{-1} \leq |2J| \leq 2000$ cm^{-1}. With $|2J|$ below 900 cm^{-1}, an excess of dimers with thermally occupied triplet states is present, giving rise to the line-broadening effects. At the other extreme; that is, with $|2J|$ above 2000 cm^{-1}, the number of triplet states vanishes rapidly, and no ZFS features are detected. These benchmark values are subject to modification as more-extensive numerical data on the exchange interactions in thiazyl radical pairs become available.

3.6. Magnetic Properties of 8 and 8SbF$_6$. In our preliminary communication, diradical **8** was reported to be essentially diamagnetic in the solid state.[15] Observed diamagnetism can be interpreted as a result of a very strong antiferromagnetic coupling between two isomeric rings via a cofacial $\pi^*-\pi^*$ overlap of the corresponding SOMOs (Figure 1, the SOMOs are shown in Figure 16). We observed that grinding of a polycrystalline sample of $[\mathbf{8}]_2$ resulted in a slight increase of paramagnetism as shown in Figure 14. Both sets of magnetic data (for ground and pristine samples) can be fitted to the modified Curie law, and the extracted parameters are compiled in Table 7. The Curie constant and

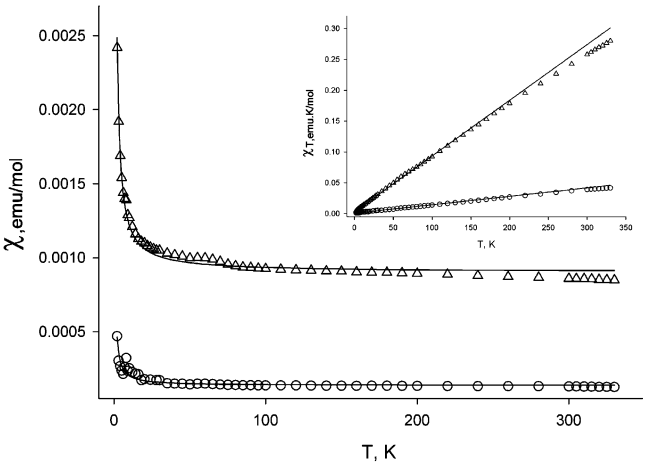

Figure 14. Temperature dependences of the χ and χT (inset) of $[\mathbf{8}]_2$ before (o) and after (Δ) grinding and their fits (—) to the Curie law, with an included TIP term ($\chi = C/T +$ TIP). Fitted parameters are given in Table 7. The actual numerical magnetic data of both samples are given in Table S2 in the Supporting Information.

Table 7. Parameters Obtained from the Fits of the Magnetic Data for Pristine and Ground Samples of $[\mathbf{8}]_2$ and Sample of $\mathbf{8}SbF_6$ to the Curie Law Modified with the TIP Term ($\chi = C/T +$ TIP)[37]

sample of $[\mathbf{8}]_2$	C, emu·K/mol	TIP, emu/mol	Estimated percentage of lattice-defect sites, % [a]
pristine	$6.5(3) \times 10^{-4}$	$1.3(1) \times 10^{-4}$	0.087(1)
ground	$3.2(1) \times 10^{-3}$	$9.0(1) \times 10^{-4}$	0.43(1)
sample of $\mathbf{8}SbF_6$	$7.5(3) \times 10^{-4}$	$8.9(1) \times 10^{-4}$	0.20(1)

[a] Calculated as C/0.75 for **8** and C/0.375 for $\mathbf{8}SbF_6$, where 0.75 and 0.375 are the Curie constants for an ideal disjoint diradical and isolated $S = {}^1/_2$ spin, respectively.

the temperature-independent paramagnetism (TIP) term are higher for the ground sample by about 1 order of magnitude, reflecting the larger magnetic response of this sample. One could surmise that this behavior is caused by Pauli paramagnetism,[51] arising from the polarization of spins at the

(48) (a) Metzger, R. M.; Heimer, N. E.; Gundel, D.; Sixl, H.; Harms, R.; Keller, H. J.; Nöthe, D.; Wehe, D. *J. Chem. Phys.* **1982**, *77*, 6203. (b) Azcondo, T.; Ballester, L.; Golhen, S.; Gutierrez, A.; Ouahba, L.; Yartsev, S.; Delhaes, P. *J. Mater. Chem.* **1999**, *6*, 1237. (c) Johnson, M. T.; Arif, A. M.; Miller, J. S. *Eur. J. Inorg. Chem.* **2000**, 1781.

(49) (a) Miller, J. S.; Krusic, P. J.; Dixon, D. A.; Reiff, W. M.; Zhang, J. H.; Anderson, E. C.; Epstein, A. J. *J. Am. Chem. Soc.* **1986**, *108*, 4459. (b) Mayerle, J. J.; Torrance, J. B. *Bull. Chem. Soc. Jpn.* **1981**, *54*, 3170.

(50) Lü, J.-M.; Rosokha, S. V.; Kochi, J. K. *J. Am. Chem. Soc.* **2003**, *125*, 12161.

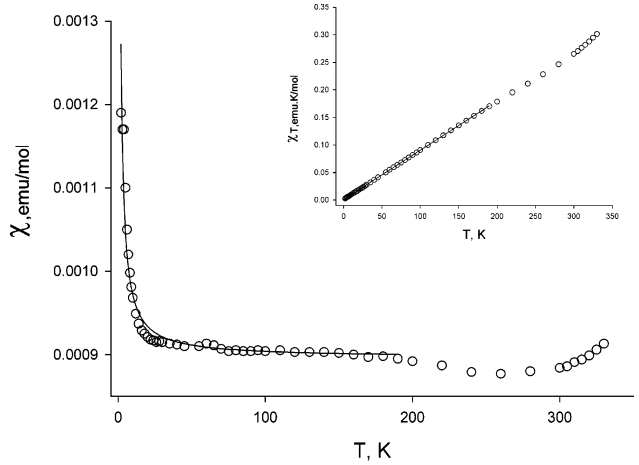

Figure 15. Temperature dependence of the χ and χT (inset) of **8**SbF_6 and their fits (—) to the Curie law with an included TIP term ($\chi = C/T +$ TIP). The data were fitted only below 190 K. Fitted parameters are given in Table 7. The actual numerical magnetic data are given in Table S3 in the Supporting Information.

Fermi level in the ground sample, although the dimerization of **8** suggests Mott insulating behavior. Alternatively, we cannot discount the introduction of ferromagnetic impurities upon the grinding process. At present, we do not have a definitive explanation for the observed increase in magnetism.

The magnetic data of **8**SbF_6 are presented in Figure 15. This salt is also diamagnetic in the solid state, containing only 0.20(1)% paramagnetic defects. Strong antiferromagnetic interaction observed in **8**SbF_6 is due to the formation of face-to-face dimers as described in Section 3.2.2. (Figure 3) and is consistent with the solid-state EPR measurements performed on this sample (Section 3.5.3.). However, there is a steady increase of χ at higher temperatures (above 300 K), the feature that is absent in the magnetic data of **8**. This observation suggests that the magnitude of the antiferromagnetic interaction in $[\mathbf{8}^{\bullet+}]_2$ is likely weaker than that in $[\mathbf{8}]_2$. Fitting the magnetic data of **8**SbF_6 to the Bleaney—Bowers equation[36] did not allow the extraction of any meaningful values of magnetic exchange interaction ($2J$) because of a very large uncertainty in this parameter. The singlet—triplet gap of $[\mathbf{8}^{\bullet+}]_2$ was determined from solid-state variable-temperature EPR studies to be -1800 ± 100 cm^{-1} -23 ± 1 kJ/mol (Section 3.5.3.). Such a large antiferromagnetic exchange interaction causes a rather weak magnetic response of the sample, for which the magnetic susceptibility technique is not sufficiently sensitive. On the other hand, the much more sensitive EPR technique is capable of estimating the large singlet—triplet splitting in $[\mathbf{8}^{\bullet+}]_2$, because the triplet components can be selectively integrated, whereas the magnetic susceptibility technique accounts for the overall response of the sample (lattice-defect sites + thermally occupied triplet state + TIP).

An increase of χ observed in **8**SbF_6 above 300 K is most likely a result of the dissociation of a small portion of dimers into monomers, producing the paramagnetic $S = {}^1/_2$ sites, or the further population of the triplet excited state within the radical pair manifold. Similar effects have been very well documented by Oakley and co-workers for analogous thiazyl radical dimers,[35,38] including dimeric diradical **10**,[14b] implying the expediency of the solid-state EPR studies of these and related thiazyl radical dimers.

3.7. Computational Analysis. 3.7.1. Comparison of Trends and Structures in the Series of Isolated Molecules 8, $\mathbf{8}^{\bullet+}$, and $\mathbf{8}^{2+}$. Table 2 shows a good agreement between the calculated and the experimental internal parameters of **8**, $\mathbf{8}^{\bullet+}$, and $\mathbf{8}^{2+}$. The structural trends associated with stepwise reduction of the $-CNSSN^+$ and $-CNSNS^+$ rings can be conveniently traced by comparing the calculated bond lengths of the heterocyclic NSNSC—CNSSN framework. These data are preferred to the X-ray values, because there are some relatively large standard deviations in the bond distances. To explain the observed structural changes, the frontier molecular orbitals (FMOs) of the NSNSC—CNSSN species have been analyzed (Figure 16).

The first reduction from $\mathbf{8}^{2+}$ to $\mathbf{8}^{\bullet+}$ leaves the internal parameters of the —CNSNS ring almost unchanged while lengthening the S—N and S—S bonds in the —CNSSN ring. This reduction corresponds to occupying molecular orbital (MO) 52, which is almost completely localized on the —CNSSN ring and π^* antibonding, with respect to N and S atoms of that ring.

The second reduction from $\mathbf{8}^{\bullet+}$ to **8** occupies MO 53 and changes the internal parameters of the —CNSNS ring while leaving the —CNSSN ring unaltered. This reduction elongates all of the bonds of the —CNSNS ring with the exception of C1—N1, which is shortened (causing a slight increase in the C1—N1 stretching mode, Table 1). The changes are directly related to the shape of MO 53, which has π bonding between the C1 and N1 atoms and π^* antibonding with respect to all of the other atoms of the —CNSNS ring.

No significant differences are observed in the C1—C2 bond lengths of the NSNSC—CNSSN species, with the exception of $\mathbf{8}^{2+}$, which is slightly elongated compared to the C1—C2 bonds of $\mathbf{8}^{\bullet+}$ and **8** (calcd 1.476, 1.459, and 1.466 Å, respectively). This is in accordance with the antibonding nature of HOMO 51 of $\mathbf{8}^{2+}$ and the nonbonding character of MOs 52 and 53, with negligible coefficients on the C1 and C2 atoms. This implies that the closed-shell state of **8** cannot be written as the zwitterionic quinoidal structure **12′** (Chart 4) with the C═C double bond but has some zwitterionic characteristics of the structure **12** (shown in Figure 16 and Chart 2).

Dimerization of **8** does not significantly affect the internal parameters of the isolated diradical in the solid state, which are similar to those of the corresponding monoradicals $RCNSSN^{\bullet}$ and $RCNSNS^{\bullet}$. Therefore, from the shapes of SOMOs 52 and 53, diradical **8** can be classed as pseudo-disjoint, because the SOMOs are not perfectly localized on different rings. Multiconfigurational CASPT2(8,8)/TZVPP calculations on triplet and singlet states of **8** predicted the ground state to be a singlet with an almost degenerate triplet state ($2J = -339$ cm^{-1}). Calculated structural parameters

(51) Williams, J. M.; Ferraro, J. R.; Thorn, R. J.; Carlson, K. D.; Geiser, U.; Wang, H. H.; Kini, A. M.; Whangbo, M. H. In *Organic Superconductors. Synthesis, Structure, Properties and Theory*; Grimes, R. N., Ed.; Prentice Hall: Englewood Cliffs, NJ, 1992.

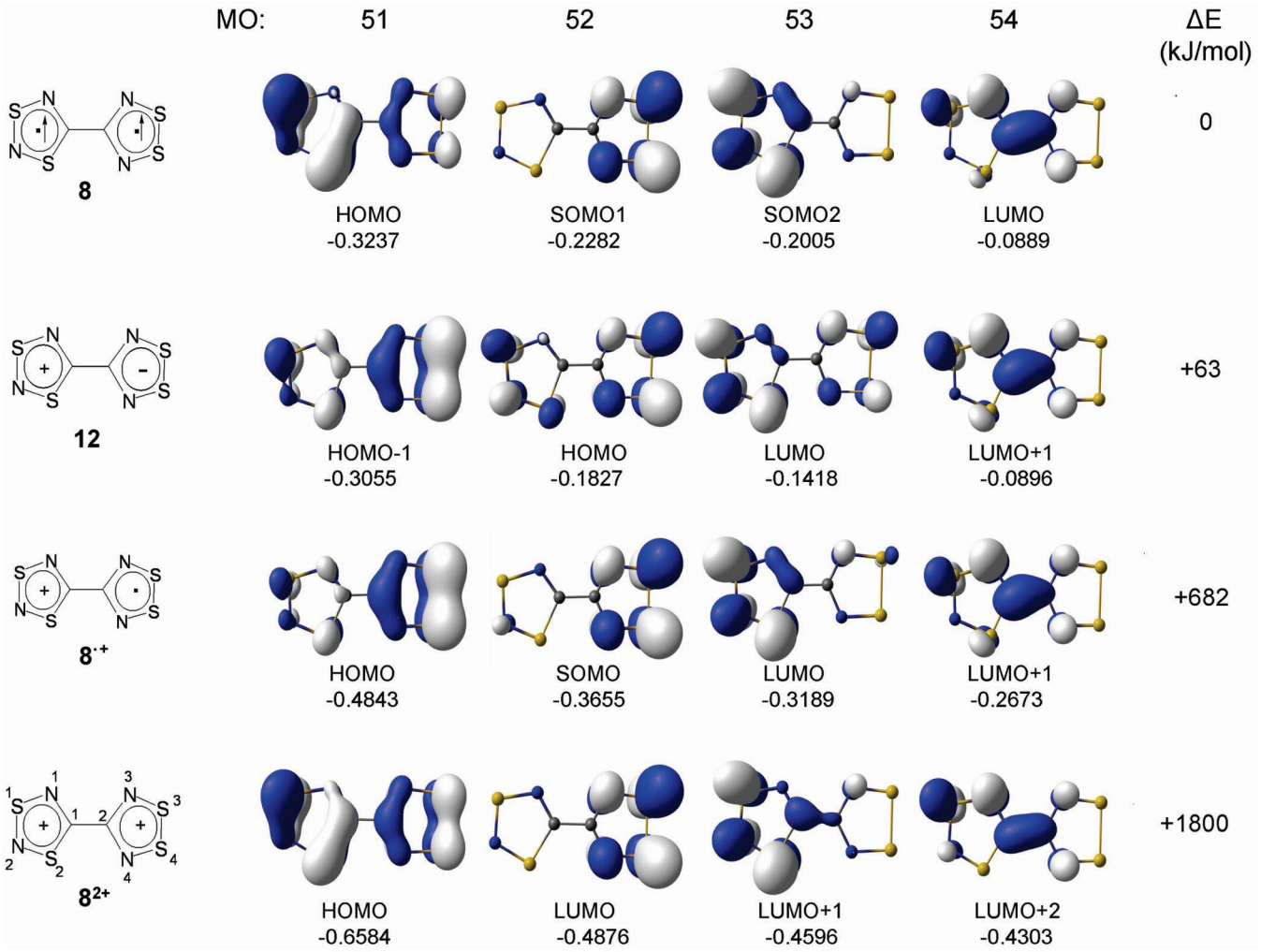

Figure 16. π MOs 51−54 and MPW1PW91/6-311+G(2df) orbital energies (hartrees) for the NSNSC−CNSSN series of molecules, drawn at the isosurface of 0.05 au.

Chart 4

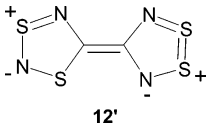

12'

of both triplet and singlet states were almost identical (Table 2), accounting for the little mixing between the two SOMOs. From the frontier orbital occupancies, we could determine that **8** possessed 81% diradical character,[39] which is close to 100%, in agreement with the frontier orbital diagram of **8**. Broken-symmetry DFT calculations gave an ST gap of -120 cm^{-1}, which is of the same order of magnitude as that of the more-robust CASPT2 method.

In comparison, previous studies have determined that **9**[13] and **10**[14b] were also disjoint radicals. An MO analysis similar to that presented in Figure 16 was performed for **9**. In the present article, we have carried out CASPT2(8,8)/TZVPP calculations on **9** and **10** and found ST gaps to be $+3$ and -269 cm^{-1}, with diradical characters of 95 and 81%, respectively. On the basis of the small ST gaps and calculated diradical characters, it can be concluded that **8**, **9**, and **10** belong to the class of disjoint diradicals with nearly 100% diradical character.

The experimental coplanar structure of NSNSC−CNSSN is expected to be the most-stable conformation with respect to rotation of the rings about the C1−C2 bond, on the basis of the previous investigations of the related diradicals **9**[13] and **11**$^{2+}$,[33b] with the exception of **10**, in which the twisted conformation [dihedral angle 10.5°, MPW1PW91/6-311G (2df)] is lower in energy than the planar structure.[13] The potential energy scan with respect to rotation of the rings about the C1−C2 bond confirms this hypothesis (Figure 17).

3.7.2. Analysis of the Dimerization Modes of 8•+. Optimized conformations (starting from the geometries shown in Figure S7 in the Supporting Information) of the dimers of **8**•+ are given in Figure 18, and Table 8 summarizes calculated relative energies of $\mathbf{A_1}'-\mathbf{C_2}'$. Geometry $\mathbf{A_1}'$ of C_i symmetry was experimentally found in the solid state (Figure 3). All of the calculated intramolecular parameters of **8**•+ in arrangement $\mathbf{A_1}'$ are similar to those observed in the solid state, but the intradimeric $\pi^*-\pi^*$, S···S, and S···N interactions are about 0.2 Å shorter. It appears that both calculated and experimental structures of $[\mathbf{8}^{\bullet+}]_2$ possess a twist angle between the two isomeric rings of about 7°, although this angle is 0° in the gas phase for an isolated molecule **8**•+. This discrepancy can be most likely attributed to the

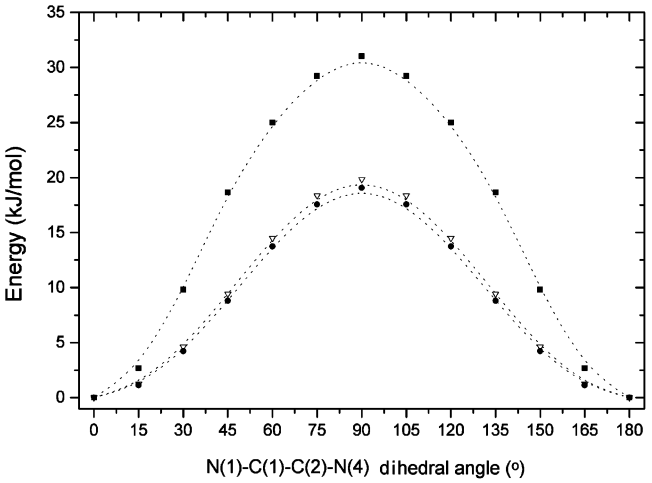

Figure 17. Calculated [MPW1PW91/6-311+G(2df)] dependence of energy on the N(1)−C(1)−C(2)−N(4) dihedral angle between the two isomeric rings for $\mathbf{8}^{2+}$ (●), $\mathbf{8}^{\bullet+}$ (■), and **8** (▽). Dashed lines are guides for the eye.

intermolecular repulsion between the $S3^{\delta+}$ and $S2'^{\delta+}$ atoms (NBO charges are +0.581 and +0.938, respectively).

Dimerization modes $\mathbf{B_1}$ and $\mathbf{B_2}$ (Figure S7 in the Supporting Information), in which the cofacial arrangement of the two radical rings is adopted (the usual dimeric conformation for 1,2,3,5-dithiadiazolyl radicals[1a,d]), transform upon optimization to $\mathbf{B_1}'$ and $\mathbf{B_2}'$ (Figure 18) to minimize the repulsive force between the two cationic moieties. Of all the conformations, $\mathbf{C_1}'$ is the most stable in the gas phase. Structure $\mathbf{A_1}'$, which is experimentally found in the solid state (Figure 3), lies 33 kJ/mol higher in energy. This difference stems from the larger repulsive interaction between the two positively charged $-CNSNS^+$ fragments in $\mathbf{A_1}'$, as compared to all of the other conformations (except $\mathbf{A_2}'$). It is possible that in the solid state the unfavorable repulsion term in the conformation $\mathbf{A_1}'$ is offset by the favorable cation−anion attraction terms, which may allow a greater lattice energy for the salt of $\mathbf{A_1}'$. We note that $\mathbf{A_1}'$ has the highest-calculated singlet−triplet gap (-3250 cm^{-1}), which is about twice that of the experimentally determined value (-1800 cm^{-1}), consistent with the highest intrinsic dimerization energy in the electrostatic field experienced in the solid state.

3.7.3. Analysis of Dimerization Modes of 8. Calculations showed that conformation **A** of $[\mathbf{8}]_2$ observed in the solid state was the most stable of all of the cofacial isomers in the gas phase (Figure 19, Table 8). There was a satisfactory agreement between the calculated and experimental intramolecular dimensions (Table S4 in the Supporting Information) and interradical contacts [exptl/calcd (Å): S1···S4′, 3.011(9)/3.166; S3···N2′, 3.022(8)/2.758; S2···N3′, 3.111(9)/2.934]. A slight deviation from planarity in **A** as compared to the experimental geometry (Figure 1) may reflect the significance of packing forces in the solid state and the inability of the gas-phase calculations to account for these effects.

The calculated singlet−triplet gap of conformation **A** is higher than that of **B** and **C** (Table 8). Thus, dimerization mode **A** ensures the maximum bonding energy between two monomers. A large magnitude of the calculated singlet−triplet gap (-8119 cm^{-1}) accounts for the diamagnetism of **8**, the absence of triplet excitons in the solid state (Section 3.5.3.), and the fact that the spin pairing interaction in $[\mathbf{8}]_2$ is primarily intermolecular.

3.7.4. Diradical Characters of Multicentered $\pi^*-\pi^*$ Bonds in $[\mathbf{8}^{\bullet+}]_2$ and $[\mathbf{8}]_2$. Dimerization in both $[\mathbf{8}^{\bullet+}]_2$ and $[\mathbf{8}]_2$ occurs via a bonding $\pi^*-\pi^*$ overlap between the corresponding SOMOs with relatively long intermolecular S···S and S···N distances. Given the relatively moderate experimentally determined ST gap of $[\mathbf{8}^{\bullet+}]_2$ (-1800 cm^{-1}), one can envisage a considerable open-shell character of these two-electron multicentered weak interactions. As described in a recent account,[11b] a multiconfigurational method appears to be most appropriate for examining the electronic nature of such weak bonds. Herein, we adopted the same computational algorithm and used the CASSCF(6,6)/6-31G* method for calculating the natural orbital occupation numbers[40] of the frontier orbitals of $[\mathbf{8}^{\bullet+}]_2$ and $[\mathbf{8}]_2$ with the geometries taken from the X-ray structure.[41] This gave estimations for the diradical characters of $[\mathbf{8}^{\bullet+}]_2$ and $[\mathbf{8}]_2$ of 39 and 31%, respectively. Interestingly, these numbers are intermediate compared to those expected for a pure closed-shell singlet state (diradical character = 0%) and a pure open-shell singlet state (diradical character = 100%). In this regard, the electronic state of both $[\mathbf{8}^{\bullet+}]_2$ and $[\mathbf{8}]_2$ can be described as diradicaloid, as has recently been proposed for a number of heterocyclic systems (e.g., $Cl_2C_2P_2R_2$,[42a] $R_4P_2B_2R'_2$,[42b] $R_2Ge_2N_2R'_2$,[42c] $Cl_2Sn_2N_2R_2$,[42d] and S_2N_2[42e]) of current interest. Previously, we concluded that the same description is more appropriate for dimer $[ClCNSSS^{\bullet+}]_2$[11a] and radical pairs $[RCNSSS^{\bullet+}]_2$ found in polymeric arrays $[C_xF_{2x}CNSSS^{\bullet+}]_n$ ($x = 2, 4$)[11b] with estimated diradical characters of 32, 45, and 36%, respectively.[11b]

We note that there are many organic radicals and radical ions that exhibit dimerization through a two-electron multicentered $\pi-\pi$ overlap. In addition to numerous examples of thiazyl radical dimers,[1] these include phenalenyl[43a] and perchlorophenalenyl,[43b] diazaphenalenyl,[43c] tetrathiafulvalenium, $TTF^{\bullet+}$,[44a] terthiophenium,[44b] and related π dimers of sulfur cations,[44c,d] tetramethylphenylenediammonium, $TMPD^{\bullet+}$,[45] tetracyanoethylenide $TCNE^{\bullet-}$,[46] tetracyanoquinodimethanide $TCNQ^{\bullet-}$[47] and its tetrafluoro analog,[48] dichlorodicyanobenzoquinonide, $DDQ^{\bullet-}$,[49] as well as other quinoidal based radical anions.[50]

4. Conclusions

In this article, we have presented an extensive experimental and computational study of the series **8**, $\mathbf{8}AsF_6$, and $\mathbf{8}[AsF_6]_2$, containing the NSNSC−CNSSN manifold with the two isomeric rings joined by a C−C single bond. $\mathbf{8}^{2+}$, $\mathbf{8}^{\bullet+}$, and **8** belong to the series of nine derivatives (given in Scheme 1 of ref 12a) formally obtainable from $\mathbf{9}^{2+}$ by reduction, isomerization, and reoxidation. These three derivatives were almost fully characterized in the present article, and the formation of $\mathbf{9}^{\bullet+}$ was evidenced from CV experiments (in addition to the EPR evidence reported in ref 12a). Previously, dication $\mathbf{9}^{2+}$ [12] and the neutral diradicals **9**[13] and **10**[14] were extensively characterized, although a single crystal X-ray

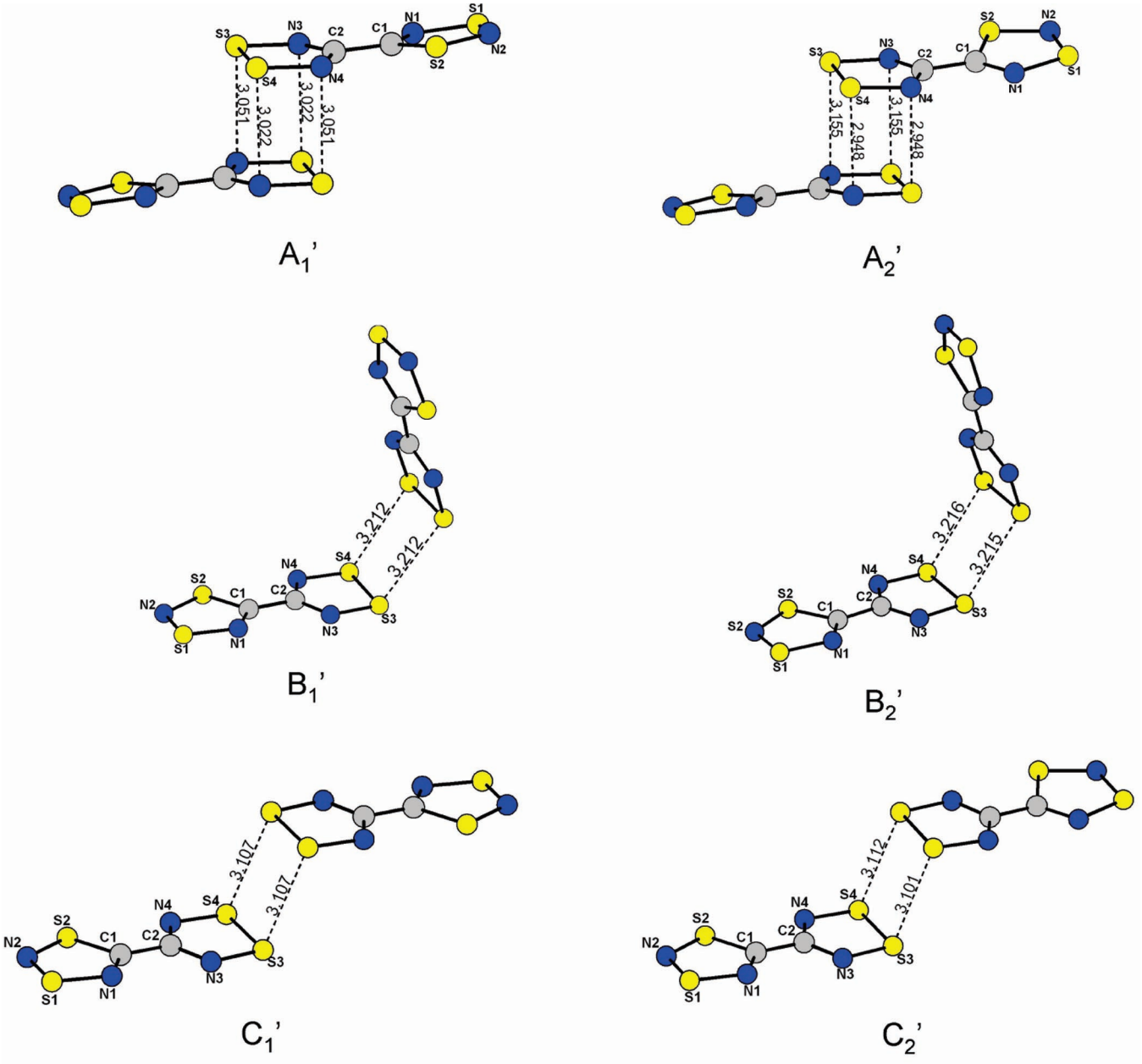

Figure 18. Optimized geometries of the conformations of $[\mathbf{8}^{\bullet+}]_2$.

structure of **9** (X-ray powder diffraction only) was elusive. A family of diradicals **8**, **9**,[13] **10**,[14] and the isolobal **11**$^{2+}$ [10a,b,33] (Chart 2) are unique in that they contain two radical rings joined by a C−C single bond and do not adopt classical Lewis structures, but like O_2, they have a thermodynamic preference for structures containing two unpaired electrons. Thus, the only two missing members in the sequence of nine derivatives (given in Scheme 1 of ref 12a) are dication **10**$^{2+}$ and radical cation **10**$^{\bullet+}$. We note that the isolation of the latter is not likely, given the presence of only one oxidation−reduction peak in the CV of **10**$^{2+}$.[14b]

Hypothetically, diradical **8** is obtained by the reduction of **8**$^{2+}$ when an unpaired electron is transferred stepwise on each of the rings. Using vibrational spectroscopy, X-ray structural analysis, and EPR spectroscopy, backed up by quantum mechanical calculations, we have shown that, upon reduction, the electronic properties of the isomeric rings

Table 8. Relative Energies and Singlet−Triplet Gaps[a] of **A**$_1$′−**C**$_2$′ Calculated Using the MPW1PW1/6-31G* Level of Theory[b]

$[\mathbf{8}^{\bullet+}]_2$ conformation	relative energy (kJ/mol)	ST gap[c] (cm^{-1})	QT gap[c] (cm^{-1})	point group
A$_1$′	+33.0	−3249(−39)		C_i
A$_2$′	+33.5	−3069(−37)		C_2
B$_1$′	+20.7	−71(−0.85)		C_2
B$_2$′	+21.3	−27(−0.32)		C_s
C$_1$′	0.00	−2393(−29)		C_i
C$_2$′	+0.31	−2383(−28.6)		C_2
$[\mathbf{8}]_2$ conformation				
A	0.00	−8119(−97)	−1895(−23)	C_i
B	+26.8	−4056(−49)	−11822(−142)	C_s
C	+38.0	−3175(−38)	−3820(−46)	C_2

[a] Negative values of singlet−triplet (ST) and quintet-triplet (QT) gaps indicate a low-spin ground state. [b] All of the calculated structures were minima as indicated by vibrational frequency analysis. [c] The values given in brackets are in kJ/mol.

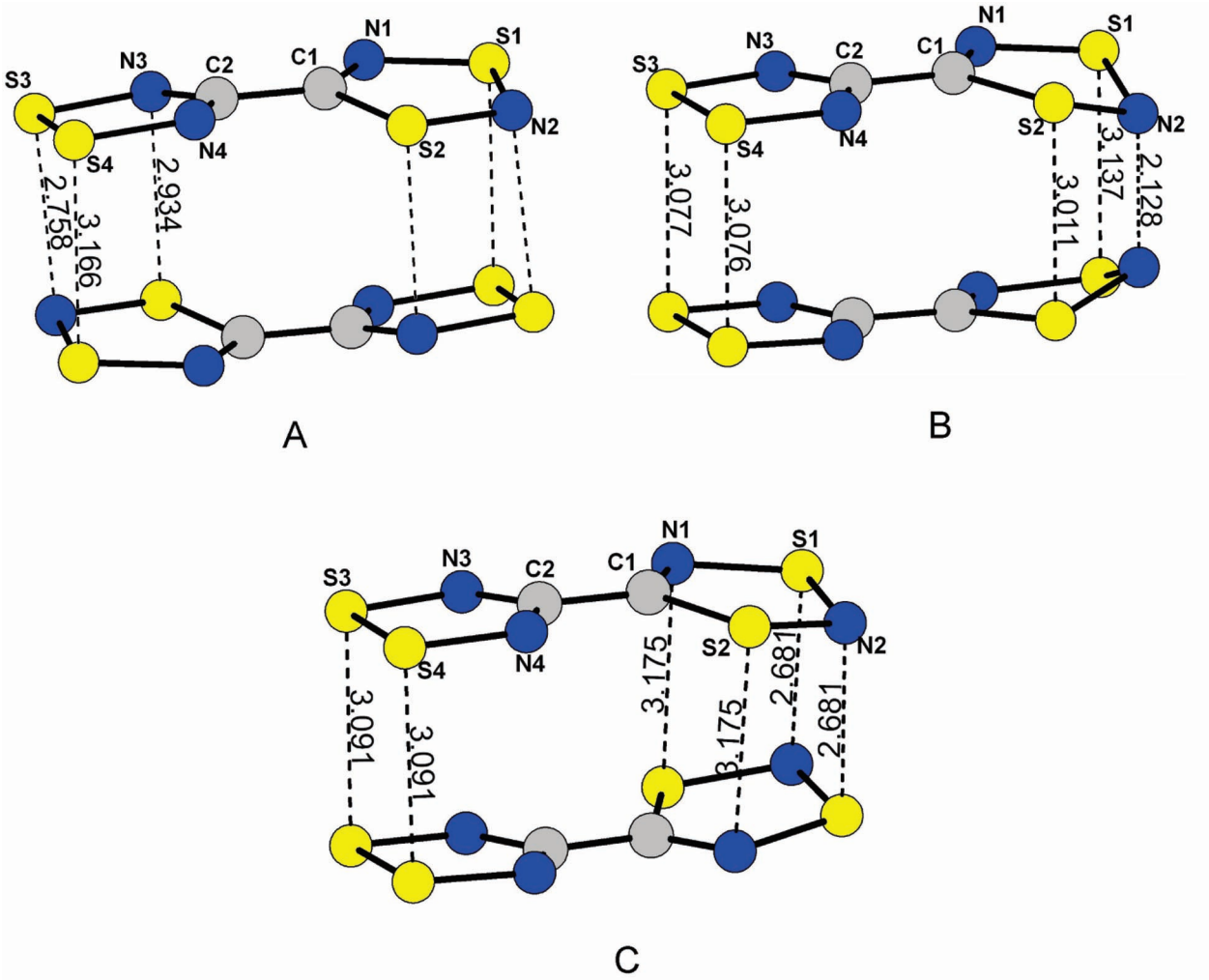

Figure 19. Optimized (MPW1PW91/6-31G*) conformations of $[\mathbf{8}]_2$.

undergo major changes. These changes seem to occur relatively independent of one another in different rings, and the two rings can be viewed as isolated moieties to the first order of approximation. However, some interactions between the two isomeric rings exist as evidenced from the electrochemical measurements of $\mathbf{8}^{\bullet+}$. Computational analysis of the electronic structure of diradical **8** indicates that it is pseudo-disjoint in nature, although we were not able to obtain direct experimental evidence for weak communication between the unpaired electrons by EPR. Notably, in solution, **8** is thermodynamically unstable with respect to symmetric analog **10**, but it is kinetically stable in the solid state and isolable because of its very low solubility in SO_2.

Although we were not able to suppress dimerization of the $-$CNSSN$^{\bullet}$ radical by incorporating positively charged group $-$CNSNS^{+}, we have shown that this group prevents the cis cofacial conformation of the two radical cations, in which there is likely to be a relatively efficient orbital overlap, and leads to the trans cofacial configuration with relatively long S$\cdots$S and S$\cdots$N linkages. This, in turn, results in the observation of the thermally excited triplet state in radical pair $[\mathbf{8}^{\bullet+}]_2$ in the solid state. Thermally excited triplet states have previously been observed for the two other thiazyl radical dimers;[11] however, $[\mathbf{8}^{\bullet+}]_2$ is the first example of a 1,2,3,5-dithiadiazolyl radical dimer to exhibit such a phenomenon. The determined in situ (i.e., in the average crystal field of the solid) singlet$-$triplet gap of radical pair $[\mathbf{8}^{\bullet+}]_2$ was -1800 ± 100 cm^{-1}, indicating that the radical cations are only weakly dimerized. We can estimate the dimerization energy of $\mathbf{8}^{\bullet+}$ to be half of the singlet$-$triplet gap; that is, ~ -11 kJ/mol. This is significantly lower than the solution dimerization energy of ca. -35 kJ/mol determined for PhCNSSN$^{\bullet}$.[31b] Thus, in the cases where the excited triplet state can be directly observable in a dimer, the solid-state EPR technique is a valuable tool that allows us to obtain in situ dimerization energies that are nontrivial to be obtained in solution.[4a$-$c] This approach can be potentially applied to the other known thiazyl radical dimers.[1a,d]

We note that in both $[\mathbf{8}^{\bullet+}]_2$ and $[\mathbf{8}]_2$ dimers, the weak two-electron multicentered $\pi^*-\pi^*$ bonds possess considerable diradical characters calculated to be 39 and 31% using the multiconfigurational CASSCF approach. Although thiazyl radicals have long been known to form weakly bound radical pairs,[1a,d] in this account we point out that the electronic nature of these bonds cannot be regarded as purely closed shell, as has been described hitherto,[1d] but most likely lies on the border between closed-shell and open-shell systems. The close analogy between these weak multicentered $\pi^*-\pi^*$

interactions and those observed for other organic−radical ions, particularly, $TTF^{\bullet+}$, $TCNE^{\bullet-}$, $TCNQ^{\bullet-}$, $DDQ^{\bullet-}$, and related species, suggest that the same description is also justified in the latter cases.

Our present findings may stimulate further interest in the well-investigated class of thiazyl radical dimers and various organic−radical ion pairs, both from experimental (e.g., characterization of the electronic structure of dimers) and theoretical (analysis of the diradicaloid ground states) perspectives.

Acknowledgment. Funding of this work was provided by NSERC (J.P., K.V.S., L.K.T.). We thank Prof. Saba Mattar (University of New Brunswick) for recording isotropic-solution EPR spectra of **8** and Dr. Martin Lemaire for assisting with magnetic measurements at Memorial University of Newfoundland. We are also grateful to Prof. Fritz Grein (University of New Brunswick) for helpful discussions. Assistance from Prof. Andrey Zibarev and Dr. Alexander Makarov as well as the staff of the laboratory of microanalysis (Novosibirsk Institute of Organic Chemistry, Novosibirsk, Russia) in carrying out the elemental analysis of **8**AsF_6 is gratefully acknowledged.

Supporting Information Available: Crystallographic data in CIF format, figures illustrating packing motifs of **8**SbF_6 and **8**$[AsF_6]_2$, decay of **8** upon rearrangement, mixed C−C/C−N vibrational modes of $\mathbf{8}-\mathbf{8}^{2+}$, dimerization modes of $[\mathbf{8}^{\bullet+}]_2$ used as inputs for quantum-chemical calculations, simulated EPR spectra of **8**SbF_6 and **8**, actual vibrational spectra of the reported compounds, and tables of various values of the reported compounds. This material is available free of charge via the Internet at http://pubs.acs.org.

IC700638N